

REPORT NO.
ITR-18-001

TITLE

Development of HTS Current Leads for the ITER Project

AUTHOR/AUTHORS

Pierre Bauer, Superconductor Engineer

AUTHOR EMAIL(S)

Pierre.Bauer@iter.org

DATE

28 February 2018



The views and opinions expressed herein do not necessarily reflect those of the ITER Organization.

© 2018, ITER Organization

www.iter.org



This work is licensed under the Creative Commons Attribution-NonCommercial-NoDerivs 3.0 IGO-ported license. (CC BY-NC-ND 3.0 IGO) You are free to share this work (copy, distribute and transmit) under the following conditions: you must give credit to the ITER Organization, you cannot use the work for commercial purposes and you cannot modify it. For a full copy of this license visit: <https://creativecommons.org/licenses/by-nc-nd/3.0/igo/>.

Development of HTS Current Leads for the ITER Project



This work is licensed under the Creative Commons Attribution-NonCommercial-NoDerivs 3.0 IGO-ported license. (CC BY-NC-ND 3.0 IGO) You are free to share this work (copy, distribute and transmit) under the following conditions: you must give credit to the ITER Organization, you cannot use the work for commercial purposes and you cannot modify it. For a full copy of this license visit: <https://creativecommons.org/licenses/by-nc-nd/3.0/igo/>.

Development of HTS Current Leads for the ITER Project

ITER TECHNICAL REPORT

P. Bauer

ITER Organization, Magnet Division,
Route de Vinon-sur-Verdon - CS 90 046
13067 St. Paul Lez Durance Cedex France

Abstract. The HTS current leads for the ITER project will be the largest ever operated, with unprecedented currents, up to 68 kA and voltages, up to 14 kV. According to the ITER agreement these leads will be provided in-kind by the PR of China. After an extensive development program at the Hefei Institute of Plasma Physics (ASIPP) and with the support of the ITER HTS working group, the ITER current leads were designed and qualified. The following discusses the main highlights of this development, with particular emphasis on the description of the design of the different types of ITER current leads and their final qualification in dedicated cold tests in nominal conditions.

Contents

1. Introduction.....	4
1.1. Background	5
1.2. Saving Cost.....	6
1.3. BiSCCO vs ReBCO	7
2. The Design of the ITER HTS Current Leads	7
2.1. Design Specifications	7
2.2. HTS Shunt and LTS Linker	9
2.3. Heat Exchanger	11
2.4. RT Terminal and Flange Assembly	12
2.5. Electron-beam Welding, Insulation, Instrumentation and Interfaces.....	14
2.6. Qualification Parameters.....	15
3. Numerical Models.....	15
3.1. 3D CFD Model (CERN)	15
3.2. Other 3D Models.....	16
3.3. 1D Models.....	19
4. Qualification.....	21
4.1. Mock-ups.....	23
4.2. Prototype Manufacture.....	30
4.3. Prototype Testing.....	32
5. Next Steps	43
5.1. Quality Assurance for Series Manufacturing	43
5.2. Integrated System Test.....	44
5.3. Some Thoughts on Operation.....	44
6. Conclusions	45
7. References	46

Acronyms

CC	Correction Coil
CIC	Cable in Conduit (conductor)
CL	Current Lead
CS	Central Solenoid
CFD	Coupled Fluid Dynamics
CTB	Coil Terminal Box
(CN)DA	(China) Domestic Agency
DB	Dry Box
DC	Direct Current
EBW	Electron Beam Welding
FE	Finite Element
G1/G2	Generation 1/2 (material)
GK	Glass-Kapton (compounded insulation)
GHe	Gaseous Helium
HPC	High Performance Computing
HTS	High Temperature Superconductor
HV	High Voltage
HX	Heat eXchanger
IB	Insulation Break
IO	ITER Organization
LHe	Liquid Helium
LN2	Liquid Nitrogen
LOFA	Loss Of Flow Accident
LTS	Low Temperature Superconductor
MDB	Manufacturing DataBase
MIP	Manufacturing and Inspection Plan
NDT/NDE	Non Destructive Testing / Non Destructive Examination
OD	Outer Diameter
OFE Cu	Oxygen Free Electronic copper
OH	Over-Heating (time)
PA	Procurement Arrangement
PD	Partial Discharge
PF(C)	Poloidal Field (Coil)
PID	Proportional-Integral-Differential (controller)
PLC	Programmable Logic Controller
PPS	Production Proof Sampling
PT	Penetrant Testing
QA/QC	Quality Assurance / Quality Control
RRR	Residual Resistivity Ratio
RT	Room Temperature
SHe	Supercritical Helium
SPC	Statistical Process Control
TB(J)	Twin Box (Joint)
TF(C)	Toroidal Field (Coil)
UT	Ultrasonic Testing

1. Introduction

The ITER project to demonstrate the feasibility of power generation by nuclear fusion technology, now under construction in the South of France, requires very large superconducting magnets for control of the burning plasma. These large coils - 18 Toroidal Field Coils (TFC), six Central Solenoid (CS) modules, six Poloidal Field Coils (PFC) and 18 Correction Coils (CC) – are supplied with 60 current leads, ranging from very large (68 kA for the TF) to medium (10 kA for the CC), transferring up to 2.6 MA into and out of the cryogenic environment (Table 1).

Based on a so-called “hybrid” design, i.e. combining superconducting and resistive sections, their main design features are derived from early prototypes and from the HTS current leads developed for the LHC project. They use gaseous helium (GHe) to cool the resistive section between an intermediate temperature and room temperature and indirect cooling of the HTS section from the 5 K cold end. The largest (TF-type) leads are over 3 m long and weigh 600 kg. The ITER current leads are assembled horizontally into the feeders, of which they are one of the key components [ref 1]. The ITER current leads use BiSCCO2223 HTS (or Bi2223) tape. The choice of HTS will be further motivated in section 1.3. Being located at the far end of the ITER feeders (Fig. 1), the leads operate in a much lower magnetic field than the coils or the feeder busbars.

Table 1: Current leads for ITER.

	Large, steady state	Large, pulsed	Medium, pulsed
Feeder	TF	PF and CS	CC
Number of Pairs	9	12	9
Number of Spares	2	2	2
Design Current	68	52/55*	10

*operation at 55 kA possible, as a recovery action for loss of a PF coil pancake (possible due to the “two-in-hand” winding scheme of the ITER PF coils).

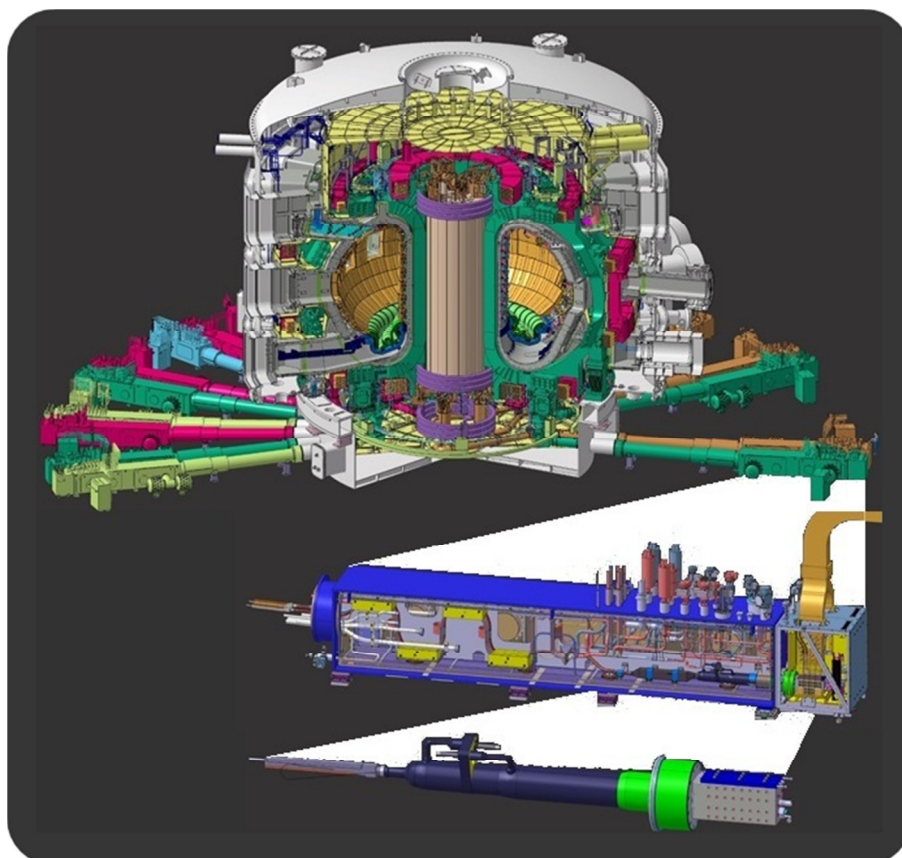


Figure 1: 3D model of the ITER Tokamak – zoom in view into feeder with current lead.

As in the case of the busbars, NbTi superconductor, comparatively cheap and easy to handle is thus the right choice for the Low Temperature Superconductor (LTS) at the 5 K end. Moreover, due to the low field the temperature margin is correspondingly greater, which justifies locating the current leads at the exit of the supercritical He (SHe) cooling circuits of the feeder system, i.e. where the SHe has absorbed the feeder heat loads prior to the cooling the base of the leads.

A well-known subtlety of hybrid HTS current leads is that it is the resistive section – the so-called Heat eXchanger (HX) - where the main design challenges lie. 1D, 2D and 3D models were developed (see further details in section 3) to optimize a number of constraints. Most importantly, however, a basic choice had to be made as there are two main categories of HX designs: type I - current carrier without fins, and type II - current carrier with fins. Type I HXs are made of thin wires, tubes or plates, and the current carrier itself has a large surface area. The HX needs less material, but the problem is to ensure that the wires/plates are cooled uniformly by the coolant flow and that the contact resistances at the two ends are both low and uniform. The current carrier of a type II HX consists of a solid Cu rod equipped with fins, which provide the functions of both heat transfer and thermal inertia. These HXs can have lower contact resistance, and enjoy the important advantage of being easier to manufacture. Possible disadvantages are higher pressure drop and shorter wetted perimeter. ITER decided to prefer the fin-type HX, also with an eye to ease of manufacture and quality control that could be applied to series production. In particular with this design, the quality (i.e. the amount of bypass flow) can be determined precisely solely on the basis of data from mechanical measurements obtained during manufacture. An efficiency of 90% can be achieved systematically with such a design, and it was felt that the risk associated with the type I HX outweighs the value of a possible gain of a few percent in efficiency.

1.1. Background

Following CERN's successful development of HTS Current Leads for the LHC [ref 2,3], several ITER parties started R&D for a HTS replacement of the conventional Cu leads, then the baseline. Among the trials was the 70 kA “demonstrator”, built by the EU party (EFDA) with KIT (then FZK) and CRPP in 2003 and tested successfully at 70 kA in 2004 in the TOSKA test facility in KIT [ref 4-8]. The original ITER current lead design proposal derived from the demonstrator [ref 7] included key technical design choices which survived into the final design. Among them is the forced flow cooling of the resistive section with 50 K helium gas taken from an intermediate cooling stage of the cryo-plant and the conduction cooling of the HTS section with SHe from the cold end. In 2004 it was decided that the Chinese ITER partner supplies the HTS leads in-kind based on a detailed (“built-to-print”) design. Finally the HTS leads were officially accepted into the ITER baseline in 2006.

ASIPP, which had recently completed the manufacture, installation and commissioning of the 16.5 kA HTS leads for the EAST Tokamak [ref 9], soon launched the manufacturing of several pre-prototypes for ITER [ref 10-17]. A 70 kA pre-prototype (“trial lead”) was tested at up to 100 kA in December 2008 using the EAST power and cryogenic infrastructure, followed by a 52 kA PF-type lead and a 10 kA CC-type lead. These pre-prototype leads explored different resistive HX designs (zig-zag vs. multi-foil) and jointing technologies (e.g. induction welded vs. soldered). Different options were also explored for the assembly of the HTS module and soldering of the internal joints. Finally key parameters such as the temperature margin in the HTS module, the time before a quench in the so-called “LOFA” condition (i.e. after interruption of the cooling gas supply) and the rate of voltage growth in the HTS during the ensuing quench were investigated and compared to model predictions. The final HTS shunt design incorporates some features of the ASIPP trial leads.

As a result of a review of the ITER HTS current leads end of 2010, the main technological design choices were finally made. Most notably it was recommended to use the type II zig-zag design for the HX as pioneered and adopted for the large scale production of the LHC leads and following which was also used in the leads of other large scale fusion plasma projects (e.g. W7X and JT60SA,[ref 18]) – as well as, of course, the 68 kA trial lead from ASIPP [ref 10]. Similarly, e-beam welding was recommended for connecting the heat exchanger to the terminal and shunt. With these decisions, the ITER project chose to employ proven techniques and designs to minimize technical risk. On the basis of these recommendations a final design was then jointly developed by ASIPP and ITER, under guidance from the HTS working group¹, a panel of experts from CERN, KIT, NIFS and other institutions. In January 2011, the ITER Organization (IO) and the Chinese Domestic Agency (CNDA) signed a Procurement Arrangement (PA), specifying the in-kind supply of the magnet feeders, including the HTS current leads, by China. The ITER feeder PA laid out a IV-phase plan for the procurement. Phase I is for the selection of the (main) suppliers, phase II is dedicated to the qualification of the manufacturing procedure and phase III to the series production. The CNDA placed a contract for the supply of the leads with the Institute for Plasma Physics of the Chinese Academy of Sciences (ASIPP) in Hefei/China in October 2011. This was followed by five years of development in preparation for the series manufacturing. This development is the subject of this note.

Although excluded from the Pressure Equipment Directive (PED - 97/23/EC), because pressure is not a design driver, the HTS current leads were effectively designed and qualified as if a PED category-1-pressure-equipment. This implies stringent requirements for the component qualification, the quality documentation (design calculations, technical drawings, manufacturing procedures, etc.) and the traceability of materials. Compliance with these requirements explains to a large extent the significant amount of time spent on the current lead development and qualification.

1.2. Saving Cost

In HTS current leads, as opposed to conventional (vapor cooled) resistive current leads, the low temperature section is designed using HTS material to reduce drastically the heat conducted into the cryogenic environment, thanks mainly to the much higher operational current density possible in the HTS superconductor. The reduced heat load justifies the use of HTS current leads as the gain in cooling cost usually outweighs the additional investment for the expensive HTS material.

When optimizing the HTS lead design the choice of the inlet temperature of the coolant, $T_{\text{He,in}}$, to the resistive HX is crucial. It determines the warm end temperature of the HTS - in the ITER current leads $T_{\text{HTS-top}}=T_{\text{He,in}}+15 \text{ K}$ - and hence the amount of HTS material required to carry the specified current. This increases exponentially as the HTS critical temperature is approached, and the cost of cooling increases with decreasing $T_{\text{He,in}}$. As shown in [ref 19] the ITER leads are operated close to the optimum cost with $T_{\text{He,in}}=50 \text{ K}$, implying a $T_{\text{HTS-top}}=65 \text{ K}$.

Applying the formalism from [ref 19] the wall-plug cost of cooling of the HTS leads (at 0.1 €/kWhr assuming 20 year operation and 50% duty-factor) as well as the Bi2223 material procurement cost (at 0.1 k€/m with 0.4 m of HTS length in the shunt) can be computed for the ITER leads as a function of $T_{\text{He,in}}$. Figure 2 shows that the cooling cost dominates by one order of magnitude near the optimum. It also shows that the optimum is “shallow”, i.e. a broad range of temperatures can be considered. The cost in Figure 2 is relative to that of cooling a conventional

¹ The HTS working group convened twelve times. All members are acknowledged at the end of this report.

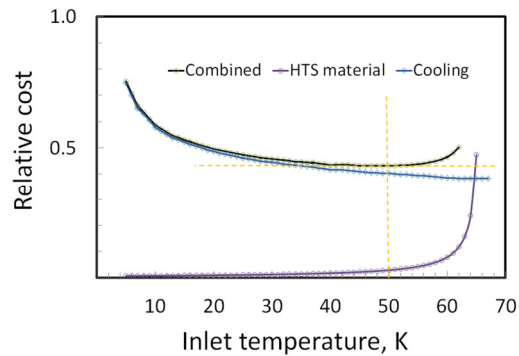


Figure 2: Cost (relative to conventional leads) for the ITER HTS current lead cooling and HTS procurement as function of resistive heat exchanger GHe inlet temperature. A design temperature margin of 10 K is accounted for in the HTS material requirement.

(vapor-cooled) current lead. As is typical for such leads [ref 20], the heat conducted to the cold end is ~ 1.2 W/kA, where it is extracted by evaporating liquid He (the heat of vaporization being 20 J/g) and the total wall-plug power required for cooling conventional ITER current leads would be ~ 3 MW. This is reduced by almost 50% with HTS leads, resulting in electricity cost savings of ~ 1 M€/yr. In ITER the additional HTS material cost of ~ 2 M€ will therefore be amortized after a few years of operation.

1.3. BiSCCO vs ReBCO

The design for the ITER HTS current leads uses Bi2223, so called Generation 1 (G1) HTS material. Second Generation (G2) HTS material based on ReBCO superconductor has now more or less fully replaced G1 material in most HTS-related applications. Already during the critical decision phase of the ITER current lead project in 2011-2014, one main supplier, Bruker, stopped its Bi2223 production, following American Superconductor who did so in 2001. It was feared that all G1 producers may soon follow suit. Although it has a lower critical temperature (90 K compared with 105 K for Bi-2223), G2 HTS has double the critical current, half as much thermal conductivity, and much higher mechanical strength for comparable quench properties. But in 2011 ReBCO tape optimized for current lead application, i.e. with a low thermal conductivity stabilizer, was not commercially available, the main issue for using G2 tapes being that the support is pre-dominantly steel, which is too resistive for good current transfer between the tapes. Recent trials show that Cu-Zn sheets can be soft-soldered on the G2 tapes, possibly providing a suitable compromise between low thermal conductivity and good tape-to-tape current transfer [ref 21]. Solutions are now also being developed for the contacts within multiple-tape stacks [ref 22], such as used in HTS leads. As explained above, ITER decided to stick with known technical solutions, to minimize risk, and therefore uses G1 HTS material.

2. The Design of the ITER HTS Current Leads

2.1. Design Specifications

The ITER HTS current lead design requirements were specified in the PA, referring to ASME Section VIII, division 2 as the main (mechanical) design code. Table 2 gives the main operational parameters for which the three types of HTS current leads are designed. These are the maximum

operational currents, the maximum voltages as well as the temperature boundary conditions for operation. A key parameter, which was changed after the design was completed is that the 50 K GHe supply conditions for the resistive heat exchanger were changed from 50 K (± 2 K) to a looser 40 K to 52 K. The implications of this change will be discussed later (section 4.3).

As shown in Figure 3 the ITER HTS current leads are assembled from three main components (from cold to warm):

- the HTS shunt / LTS-linker and joint assembly,
- the resistive Heat eXchanger (HX),
- the Room Temperature (RT) terminal block.

The HTS-shunt, LTS linker and joint assembly is the component containing the superconductor, HTS and LTS. The complexity of this assembly comes from the multiple electrical splices, from the resistive Cu section to the HTS and finally to the LTS. The (LTS) joint at the cold end, with which the current lead is connected to the feeder busbar, is of the “Twin-Box” (TB) type as used elsewhere to splice Cable-in-Conduit (CIC) conductors in the feeder system. The resistive HX is machined from a thick Cu rod, to produce a central axial conductor with radial cooling fins. It is inserted into a thin-walled steel jacket, with very tight tolerance to limit bypass gas flow. The zigzag flow of GHe cooling is obtained by clipping the radial fins on alternating sides, maximizing the heat exchange surface. The RT terminal block is designed for low current density, including in the contacts to the room temperature busbar system. The final design of the ITER HTS current leads was first published in [ref 23].

Table 2: Nominal operation parameters of the three types of ITER HTS current leads.

Parameter	TF	PF/CS	CC
Design DC current (kA)	68	55	10
Operational max DC current (kA)	68	52	10
Operational max voltage to ground (kV)	7	14	0.3
Max fault voltage to ground (kV)	19	29	3
Nominal operating temperature GHe supply to heat exchanger (K)	50		
Nominal operating pressure GHe supply to heat exchanger (MPa)	0.4		
Nominal operating temperature room temperature terminal (K)	~300		
Nominal operating temperature HTS top/warm end (K)	65		
Operating temperature HTS bottom/cold end (and LTS section) (K)	<7		
Maximum ramp-rate during pulse (kA/s)	-	20	10

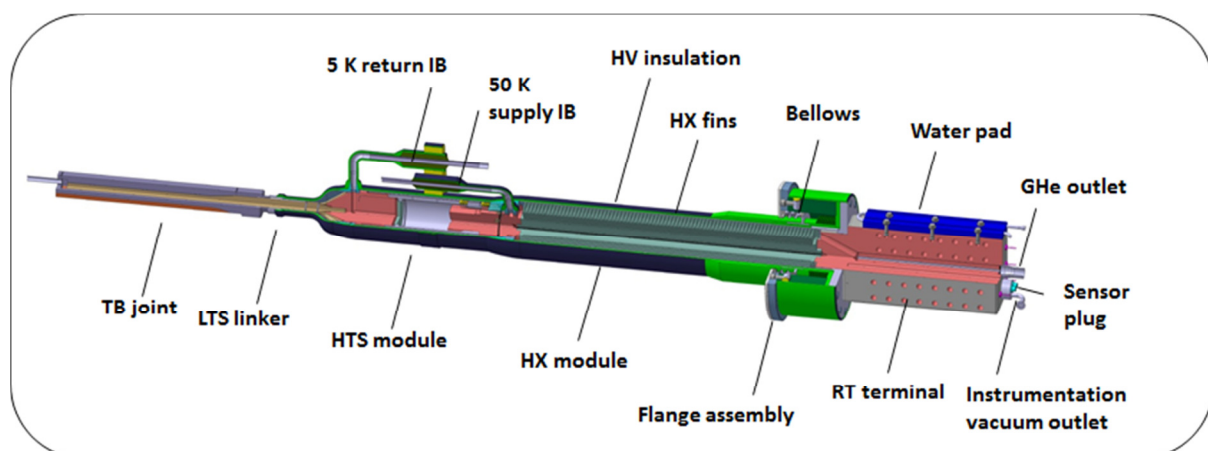


Figure 3: ITER HTS current lead design (TF-type).

2.2. HTS Shunt and LTS Linker

The shunt and linker assembly (Figure 5) bridges the temperature gap between 65 K and 5-6 K. The shunt module is composed of a thin walled stainless steel tube, which is vacuum-brazed at 830°C to two massive OFE Cu end-caps. HTS stacks are soldered into grooves along the shunt including the Cu endcaps through which the currents are transferred. The LTS linker is a ~1 m long piece of feeder CIC busbar cable terminating in a joint box that provides for connection to the feeder. It is internally cooled with SHe from the feeder busbar. A welded steel cover (3 mm thick) contains the vacuum (for the shunt section) and the SHe (for the LTS section), and gives the linker its rigidity and support. The main design criteria for the shunt/LTS assembly are related to: critical current (I_c) margin, heat leak, over-heating time² and resistances of the splices. The related specifications are listed in Table 3; further details follow in this section.

The critical current of the Ag-Au matrix / Bi-2223 tape is specified to be greater than 100 A at 77 K in self-field (this is an industry standard). The tapes are ~4 mm wide and ~0.2 mm thick, with a superconductor to matrix ratio of typically 40%. They are soldered (Sn-Ag) into stacks, which are then soldered (Pb-Sn) in vacuum into the 430/410 mm (TF-PF/CC) long Ag-coated grooves of the shunt cylinder. The use of flux is banned for the tape and stack soldering to prevent corrosion issues in the long term³. The outer diameter of the shunt is 148 mm (TF and PF) and 77 mm (CC) with an approximately regular distribution of 90 (TF/PF) and 36 (CC) stacks. The arrangement of stacks around a cylinder reduces the perpendicular magnetic field component, which lowers the HTS critical current, I_c . Neglecting this effect⁴ the number of HTS tapes required to provide the specified I_c at the operating temperature plus 10 K margin, is 1080, 900 and 180 for the TF, PF and CC type leads (corresponding to 12, 10 and 5 tapes/stack for a tape $I_c \sim 100$ A).

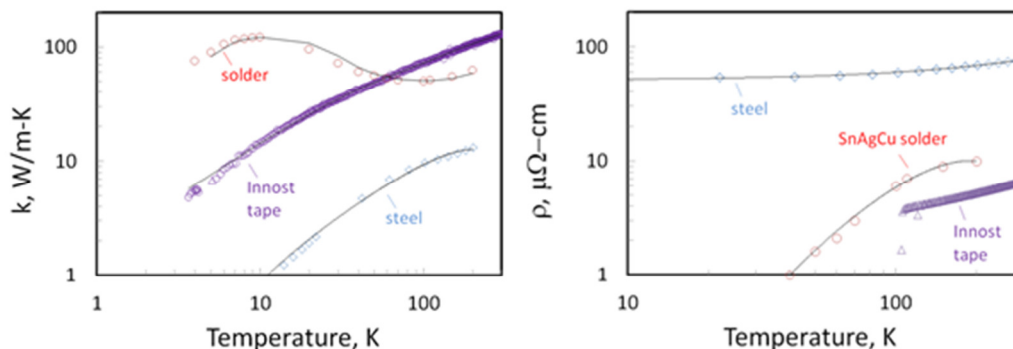


Figure 4: Thermal conductivity and electrical resistivity of Bi-2223 tape (Innost) and Sn-3.8Ag-0.7Cu solder measured by PPMS/Quantum design. Steel data from standard material reference.

² The over-heating time is the time during which the shunt can carry the full current after a quench of the HTS before reaching 200 K. It needs to be long enough to allow the current to be ramped down in the coil/feeder circuit after a quench.

³ Although the use of Pb based solder is prohibited by the European Directive 65 (2011), its use cannot be avoided, as the manufacture of the shunt and LTS linker requires a combination of soldering steps with “cascading” melting points (stacks, shunt, insulation curing). However, as for CERN’s LHC, an exemption clause of the ED65 can also be invoked for the ITER leads, as the quantity of solder is small (<1 kg compared with >10 000 tons of the TF magnet) and as the leads are part of a “large-scale-fixed installation, assembled by professionals and used permanently in a pre-defined and dedicated location and/or de-installed by professionals”.

⁴ The perpendicular self-field of an individually tested stack is larger than the field a stack sees when assembled in the lead. Using the critical current as measured in the stack test to estimate the number of stacks needed in the lead, therefore leads to an overestimation of the HTS material needed. The extra material provides critical current margin for additional operational safety. Further details on this margin can be found in section 3.2.

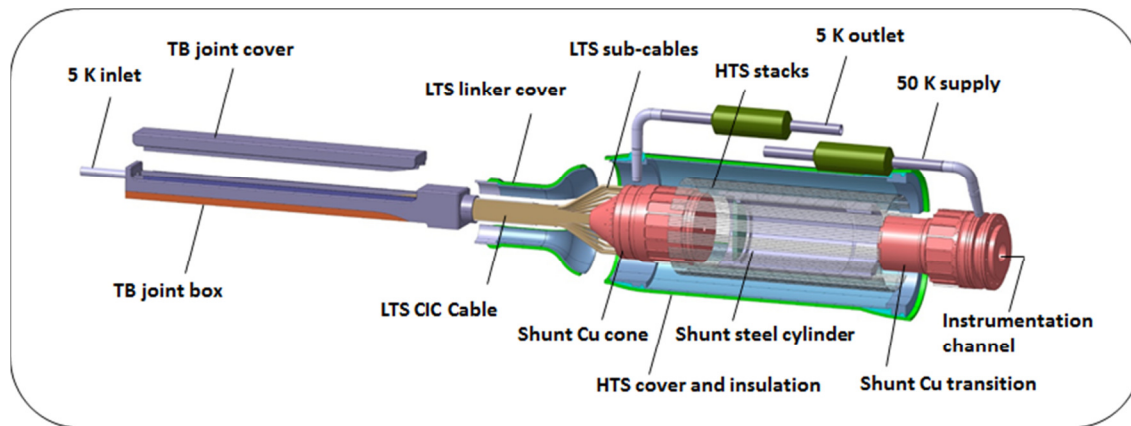


Figure 5: Shunt & LTS linker 3D model – exploded view.

The cold end of the shunt is kept at 5-6 K with a flow of SHe entering the lead via the box-joint and flowing up the linker into 29/11 holes (\varnothing 4mm/3mm) in the cold endcap of the TF/CC type. At their warm end the temperature is regulated to 65 K with the flow of 50 K GHe entering the HX for cooling of the resistive section (see section 2.3 for further details). The HTS stacks are therefore conduction cooled from the 5 K end. The Bi-tapes are specially engineered for use in HTS current leads with 3 at% (~5 w%) Au alloyed into the Ag matrix to reduce the thermal conductivity (to ~2500 W/m integrated 5-65 K, see Figure 4). Nevertheless, the Au-doped Ag matrix of the HTS tapes remains the main contributor to the shunt heat leak. The solder is the second largest contributor to the heat load; although its thermal conductivity is more than an order of magnitude larger than that of the tape, its cross-section is only ~10 %. In a TF lead with a total tape cross-section of 1000 tapes (~1000 mm²) and the length of the HTS module of 0.31 m excluding the contacts to the Cu blocks, the heat leak per lead due to the stacks is calculated to be ~10 W (counting the solder) – see section 3.3 for details on the calculation. One must add to this the smaller, albeit non-negligible contribution from the stainless steel shunt cylinder and the insulated stainless steel cover.

During a quench of the HTS, current spills over into the stainless steel cylinder. Knowing the specific heat (C_p) and electrical resistivity (ρ), the cross-section (A_{shunt}) needed to ensure the specified over-heating time, t_{OH} , can be conservatively estimated by using the adiabatic heat balance equation $A_{shunt}^2 = t_{OH} \times I_{shunt}^2 / \left(\int_{65K}^{200K} \left(\frac{C_p}{\rho} \right) dT \right)$; the ratio C_p/ρ determines the rate at which the temperature rises. The over-heating time is driven by the fraction of current flowing in the steel (I_{shunt}) as well as the steel cross-section, two parameters that are not independent as the current sharing between matrix and tape depends on the ratios of (A/ρ) of steel and tape and thus also on A_{shunt} . In the TF type lead the upper 50 mm of the steel cylinder is 20 mm thick (whereas it is 10 mm elsewhere to minimize heat conduction), i.e. the total steel cross-section is almost 10 times larger than the total stack cross-section. Since the matrix resistivity is approximately 20 times smaller in the temperature range of interest [see Figure 4], about $\frac{1}{3}$ of the current flows in the steel support during the quench. Note that the specified t_{OH} also includes a safety factor of 2 because the fast discharge of the ITER coils is actually completed in half the specified t_{OH} .

The HTS stacks extend beyond the shunt steel section to provide length for the soldered contacts to the Cu end sections. The contact length is 49 mm at the warm end and 71 mm at the cold end, taking into account the lower contact resistance at the cold end, which results in a longer current transfer length (streaming effect). At the cold end of the shunt the current transfers into the LTS sub-cables of the linker. The linker busbar cable is “splayed” into its third-stage components, i.e. 30/12 pre-soldered (Sn-Ag) sub-cables for the TF-PF/CC type leads. These pre-soldered sub-cables (i.e. of 45 strands each - 30 NbTi and 15 Cu for the TF-PF type) are then vacuum soldered

(Pb-Sn) into blind holes in the bottom Cu end of the shunt, underneath the HTS to Cu contacts. The total penetration depth into the Cu section is 120/92 mm in the TF-PF/CC type leads, i.e. about the length of the sub-cable twist pitch. The other end of the LTS linker busbar is terminated as a standard twin-box type joint, described in detail in [ref 24]. Its contact length of 450 mm is about 50 mm more than the twist pitch of the busbar cable (TF-PF type). Then the box is welded over the cable under pressure strongly compacting the cable with a layer of In foil placed between the cable and the Cu sole of the box. Further discussion of the critical current margin and overheating time (equal to that of the HTS section) of the LTS linker conductor (or feeder busbar) can be found in [ref 25].

2.3. Heat Exchanger

The resistive Cu Heat eXchanger (HX) is a section of a conventional current lead which transports current across the 300 K to 65 K temperature differential with an appropriate cross-section and counter-flow cooling to absorb the resistive heating (Figure 6). The cooling flow, 50 K GHe supplied at a pressure of 4 bar, also determines the temperature at the cold end (and thus the temperature at the warm end of the HTS). With the strong dependence of the Cu resistivity on temperature, most of the Joule heating occurs in the warmer part of the HX, so the heat flux transferred to the gas stream in the warmer part is greater than that near the cooler end. Typically the “shape factor” (i.e. the geometry) of the current carrying part is considered to be optimal when a zero temperature gradient is achieved at the RT end of the HX. The efficiency (= minimal coolant mass flow) is then obtained by a proper design of the wetted perimeter, which, in the fin-type HX design, is related to the area, thickness and spacing of the fins. These parameters, together with the size of the cut at the edge that creates the zigzag flow, determine the pressure drop, which must remain within the specified limit. The Cu cross-section must also be sufficient to provide the necessary thermal inertia for safe operation during LOFA (Loss of Flow Accident). Finally the parameter space for optimization is further constrained by practical external considerations. First, it must be possible to extract the current lead from the feeder when it is installed in the Tokamak. This operation requires the total length of the lead to be less than ~3 m. All the components have been reduced to the minimum, leading to a maximum length available for the HX of 1 m. Second, experience with the trial leads showed that the minimum practical thickness and spacing for the machining of fins is 3 mm. Finally the external diameter of the fins should ideally be chosen to match preferred sizes of the stainless steel tube that encases the HX.

The HX is made of OFE Cu with a RRR (Residual Resistance Ratio between 300 K and 4.5 K) of > 50 . As a result of Wiedemann-Franz law an optimized gas cooled lead is characterized by a fixed value of shape factor $I \times L / A \sim 10^7 \text{ A/m}$ and thus 10 A/mm^2 at 1 m length, and for which the temperature gradient is minimal at the room temperature end. Given the ensuing temperature (and thus resistivity) profile the voltage V across the HX is $\sim 80 \text{ mV}$ in this condition. Such optimum, however, can only be achieved for one current, which in this case is the DC design current. The PF and CC leads will operate in pulsed mode, but the optimization of the HX was also done for the maximum DC current condition (conservative).

Further optimization is needed for the heat transfer, but its estimation requires complex numerical models (see section 3). A rough estimate of the required cooling mass flow can be done for a TF-type HX assuming the approximate GHe enthalpy of 5.2 J/g/K and the total temp difference of (300-50) K, which gives 1300 W per g/s of mass-flow. The total Joule heating power to be extracted (neglecting heat conducted into the HX from the RT end) is $I_0 \times V \sim 5.5 \text{ kW}$, thus 4.2 g/s of GHe mass flow is required to cool the heat exchanger assuming 100% efficiency and infinite heat transfer coefficient. For a more realistic heat transfer coefficient - which from the models

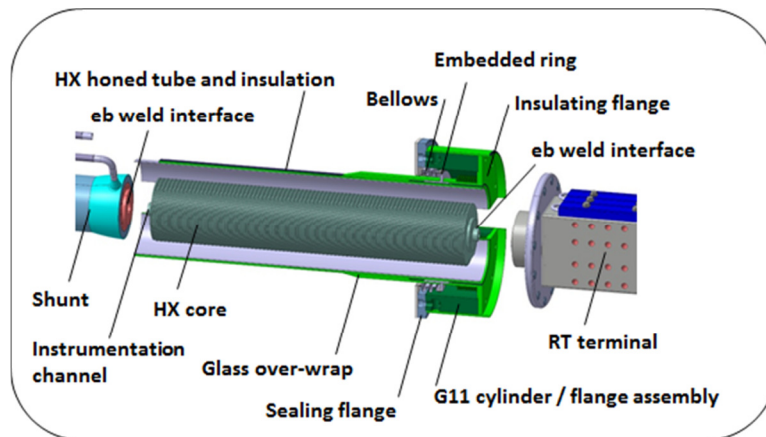


Figure 6: ITER HTS current lead heat exchanger – exploded view.

discussed in section 3 is $\sim 400 \text{ W/m}^2 \text{ K}$ for turbulent flow, approximately 14 m^2 of heat transfer area are required in a TF type lead (assuming a small temperature difference of $\sim 1 \text{ K}$ as for an efficient heat exchanger), resulting in an outer fin diameter of close to the 188 mm in the design (not counting the 92.4 mm diameter central current carrying rod). The models discussed in section 3 estimate the 50 K GHe mass flow rate for the TF/PF/CC version of this heat exchanger to be 4.4/3.5/0.6 g/s. This translates into an efficiency of $\sim 95\%$.

The contact resistance between the cold end of the HX and the HTS stacks impacts on both the performance and the optimization of the lead. The resistance between the HTS and the cold end of the HX is specified to be $< 10 \text{ n}\Omega$ (TF-type), made up of 1-3 n Ω for the joint and $\sim 8 \text{ n}\Omega$ for the Cu. This additional dissipation is cooled by the flow of 50 K helium in the channel in the so-called transition section and it will increase the required mass flow to about 4.5 g/s at full current for the 68 kA lead. Add to this the off-optimum condition at the RT terminal end (non-zero temperature gradient) which further increases the mass flow rate required. The experimental mass flow numbers required indicate a practical efficiency closer to 90% (see test results from section 4).

Using a similar adiabatic model as for the shunt - replace t_{OH} by t_{LOFA} , A_{shunt} by A_{HX} and the temperature interval 65 to 200 K, by 65 to $\sim 80 \text{ K}$ (i.e. the HTS quench temperature) and using the properties of Cu - the LOFA time is hundreds of seconds. Note that a key factor for LOFA is the additional Cu mass in the so-called “transition” region between HX and shunt, resulting in a larger “effective” A_{HX} than if considering only the HX Cu cross-section. The longer the LOFA time, the more time during ITER operation to re-establish the 50 K GHe supply and/or to start ramping down the coil current (thus avoiding a fast discharge from full current).

As discussed in further detail in section 3 the CFD models predict a pressure drop of $\sim 1.2 \text{ bar}$ for a 4.6 g/s mass flow through the TF-type HX (with a helium inlet conditions of 50 K at 4 bars), which is well below the specified limit of 2 bar (see further discussion on p-drop in sections 3 & 4). Factors in this pressure drop are the fin-to-fin spacing (3 mm) and the size of the cut at alternating sides of the fins (10 mm in the CC-type and 15 mm in the TF/PF types). The HX is enclosed in an stainless steel casing with 3 mm wall designed to withstand the specified 7 bar test pressure. A tight fit prevents the GHe bypass flow.

2.4. RT Terminal and Flange Assembly

The Room Temperature (RT) terminal (see Figure 7) is a brazed assembly made of several 316 L steel and Cu components. The main Cu block is designed for low current density (2-3 A/mm²) to limit Joule heating. Flexible RT busbars are connected to the two side surfaces, with contact

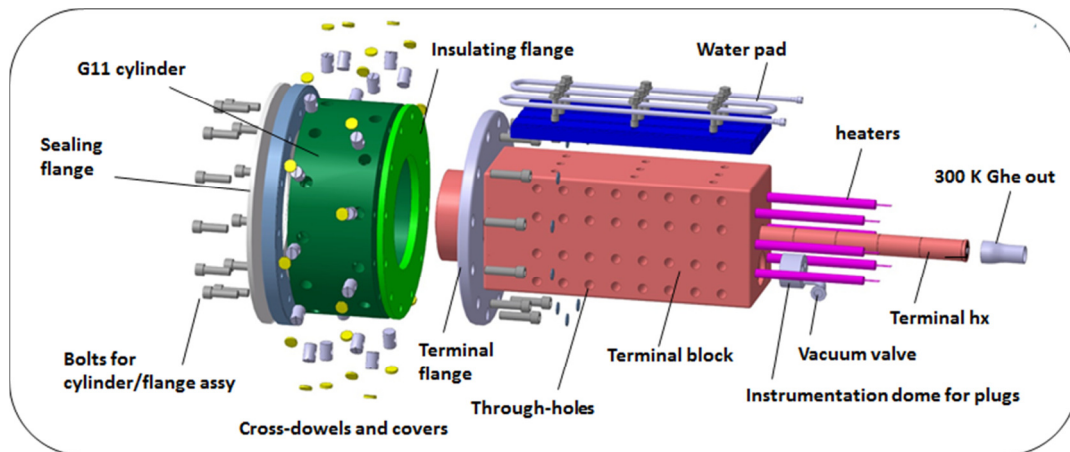


Figure 7: ITER HTS current lead RT terminal – exploded view.

surfaces limiting the contact current density to well below 0.5 A/mm^2 , a safe value. A thin Ag coating as well as care applied during bolting of the flexibles should limit the contact resistance / heating to less than $120 \text{ n}\Omega / 500 \text{ W}$ in a TF-type lead (unavoidable streaming accounts for half of this). These safe design choices result in a large size - in the TF lead, for instance, the terminal block alone weighs approximately 200 kg.

As a precautionary measure, a water-cooling pad, designed to extract 2 kW of power, is affixed to the top surface of the terminal. Additional cooling from the inside is provided by a small heat exchanger in the terminal, which extracts some residual cooling power from the GHe exiting from the HX on its path to the gas recovery outlet (this HX is designed with a very large equivalent hydraulic diameter and thus contributes very little to the pressure drop). The terminal also incorporates 6/4/2 electrical heaters in the case of the TF/PF/CC leads (500/200 W for each in the TF-PF/CC). The heater power provides the heat needed to warm up the GHe from the HX to room temperature during stand-by (zero current operation). Over-cooling of the terminals and ensuing icing is actually the more serious issue facing the terminals, potentially creating HV tracking issues due to water condensation during high voltage operation. Since the heaters are not designed to heat the full flow of GHe to room temperature in the absence of current, this will need to be prevented by proper interlocking. External mechanical support is applied via the fourth, lower, surface.

The feeder Coil Terminal Box (CTB) is at ground potential. The component of the lead that interfaces with the CTB must therefore provide insulation in ambient air between the terminal and the CTB. It must also provide mechanical support for the lead, seal the CTB vacuum. Given the large mass of the TF current lead it was decided to separate the function of mechanical support from that of the delicate insulating vacuum seal. The resulting flange design is also shown in Figure 6. A thin cylindrical stainless steel cylinder is bonded to the multilayer, epoxy-impregnated Paschen-tight insulation covering the body of the lead. This cylinder, called the embedded ring, incorporates a radial feature that protrudes from the overwrap that completes the vacuum seal; to this feature is welded a bellows that is in turn welded to the metal flange that mates up with the face of the CTB. Support for the lead is located outside the vacuum enclosure and is not subject to Paschen-tight rules. It consists of a 160 mm long, 50 mm thick G11 cylinder, fastened at one end to a stainless steel ring brazed to the terminal and at the other end to the stainless steel flange that is clamped to the end face of the CTB. In the case of the PF it has additional tracking length enhancing surface corrugations (not shown in Figure 7).

2.5. Electron-beam Welding, Insulation, Instrumentation and Interfaces

Separate machining of the HX and terminal allows for larger terminal block dimensions, thus reducing its current density providing space for installing heaters and for the connection to the warm busbars. Independent manufacturing of the shunt and linker assembly is also an advantage as it simplifies the multiple toolings for the different soldering steps. It also avoids heating the HX Cu unnecessarily (annealing would cause undesirable softening and increase of the RRR). Electron-beam welding, as pioneered by CERN for the LHC leads, was selected as the preferred technique for joining these three sub-assemblies, as it provides excellent quality joints while minimizing the heat-affected zone. This is especially an advantage for the shunt component, as the soldered HTS stacks are only 70 mm away from the weld. For the TF lead the minimum weld penetration depth is ≥ 30 mm.

The insulation is yet another critical sub-component of the ITER HTS current leads. The 30 kV test voltage is at the limit of pure glass-fiber insulation when the design margin is added (limiting field strength is ~ 15 - 16 kV/mm). The ITER feeders and HTS current leads therefore need to be insulated with a combined polyimide / impregnated glass fiber system. As GHe can leak from the CIC, the insulation system needs to be “Paschen-hard”. It also had to be unified for the entire feeder system to reduce the time and cost of qualification. Finally, the resin curing temperature needs to be relatively low ($\leq 80^\circ\text{C}$) to simplify the on-site insulation of the connections between the feeder components in the pit during assembly. The as-designed insulation resists 30 kV with a large safety factor (~ 3 - 4). It is made of a number of layers of polyimide combined with a prepreg fiberglass sheet, adding up to 6 mm as described in [ref 26]. All sharp metallic edges under the insulation are smoothed with a combination of green putty and glass cloth satin weave to facilitate applying the insulation proper, and semi-conducting tape to reduce field enhancement. A specific issue of the HTS current lead insulation is that it is the component in which the Paschen-hard, in-cryostat insulation “ends”, as the RT terminals are outside the cryostat and non-insulated. In particular the design must therefore address tracking and electric field distribution issues (“stress cone”).

The instrumentation of the current leads consists of voltage taps, doubled for redundancy, placed across the room temperature terminal, HX, HTS and LTS linker modules to detect quenching or overheating via the quench protection interlock system. Temperature sensors are mounted at the warm end of the shunt to monitor the HTS maximum temperature and provide a signal for controlling the GHe flow (as well as a secondary quench detection signal, should all voltage taps fail). Redundant temperature, pressure and flow sensors are mounted to monitor the He properties at the inlet and outlet of the SHe and HX cooling loops. These sensors, which can be installed on pipes on the low voltage side of the insulation breaks, also provide signals for the interlock system (i.e. to trigger a LOFA alarm long before the HTS quench). Both voltage tap and temperature sensor wires are at the potential of the lead (i.e. at HV) and they are routed within a central channel in the HX module to the RT terminal. In this way they do not have to “penetrate” the HV insulation thus removing a risk-factor for Paschen break-down. Since the pin-to-pin voltages are very low (a few V at the most), they can be fed out of the lead terminal with a LV feedthrough. This approach, which had been adopted for the LHC leads, simplifies installation and removal of the current leads. It was shown in the prototype tests that this arrangement also improves significantly the signal/noise ratio for the signals as the enveloping Cu HX shields the wires from electromagnetic noise.

The HTS current lead design was also constrained by its interfaces. Current densities need to be sufficiently low for the contacts between the room temperature busbars and the RT terminals. The 50 K GHe supply and exhaust conditions need to conform to specified flow, pressure and temperature ranges. Since the HTS leads are mounted horizontally into the feeders their mechanical support inside the feeders is especially critical. The water pad piping cannot be made

of Cu to prevent galvanic corrosion in combination with the Al busbar system, from which the water is supplied. As mentioned before there are also length constraints related to assembly and disassembly.

2.6. Qualification Parameters

Table 3 discusses the acceptance criteria for the HTS-CL qualification as defined in the PA (or documents referred to therein). They were all measured in the prototypes (see section 4).

Table 3: Qualification parameters of the three types of ITER HTS current leads.

Electro-mechanical	TF	PF/CS	CC
Max leak rate 50 K and 5 K hydraulic loop at test pressure* (Pa·m ³ /s)	<10 ⁻⁹		
Maximum cold end heat load per lead with HTS top at 65 K (W)	<15	<12	<3
Pressure drop in HEX section at max DC operation current (MPa)	0.11÷0.13	0.05÷0.07	0.005÷0.007
50 K GHe steady state flow-rate at max DC operation current (g/s)	4.5÷4.7	3.5÷3.7	0.6÷0.8
Nominal operating voltage HX at max DC current (mV)	<85	<80	<65
Temperature margin according to 2 mV criterion in ITER** condition (K)	>10		
LOFA time at max DC operation current according to 2 mV criterion (s)	>400		
Minimum HTS over-heating time according to the 2 mV criterion*** (s)	>15	>18	
Maximum RT terminal and interface BB contact resistance (nΩ)	<150		<350
Maximum HX to HTS joint resistance (nΩ)	<10		<25
Maximum HTS to LTS joint resistance (nΩ)	<1		<2.5
Maximum HTS-CL to feeder busbar TB joint resistance (nΩ)	<2		<5

* PED test pressure 50 K loop: 0.5 x 1.43 = 0.7 MPa, 5 K loop: 2.1 x 1.43 = 3 MPa, ** needs to include the effect of the stray magnetic field in ITER, *** OHT is the time after a quench to reach 200 K in the hot spot at max DC curr.

High Voltage	TF	PF/CS	CC
Minimum resistance to ground in hi-pot test* (GΩ)	<0.5	<0.5	<0.5
Maximum equivalent charge during PD test** (nC)	<10, no increase for 60 k cycles		
Paschen test ***	pass		

* DC test voltages 30 kV, 30 kV, 5 kV, ** AC test voltages (rms) 10 kV, 10 kV, 3 kV, *** Paschen test voltages 15 kV, 15 kV, 5 kV

3. Numerical Models

Various models were developed to support the design development of the ITER HTS current leads. The main model is the full length 3D CFD finite element model developed at CERN. Its main purpose was to support the design of the resistive heat exchanger. Other finite element 3D models were also developed for the mechanical and thermal analyses. Finally a suit of simpler and faster 1D models were developed for integrated and/or transient thermal / electro-magnetic analysis.

3.1. 3D CFD Model (CERN)

The 3D model of the HX was implemented with the Comsol Multiphysics™ non-isothermal flow module combined with heat transfer in solids. Reynolds-averaged Navier-Stokes (RANS) equations together with the k-ε turbulence model were used to represent the turbulent flow [ref 27]. In the vicinity of the walls, fluid behaviour is modelled using the “wall functions”. This approach lightens the mesh in the wall regions while properly resolving the boundary layer. Extensive mesh-studies were conducted on a short CC-type HX model (Figure 8). Finally the best compromise between accuracy and calculation time was obtained with the “Ph.Con.Nor.”, a physics-controlled mesh and predefined “normal” layers”. For the full length TF-type HX it has

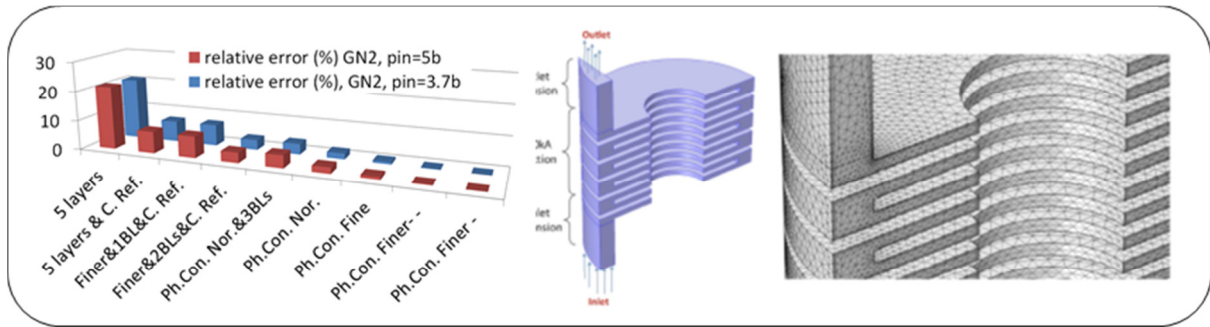


Figure 8: Mesh studies for CC-type current lead HX: Left: Plot of relative error (relative to Ph.Con.Finer). Middle: Short model of CC HX (6 cm), Right: Zoom into mesh (Ph.Con.Nor.&3BLs).

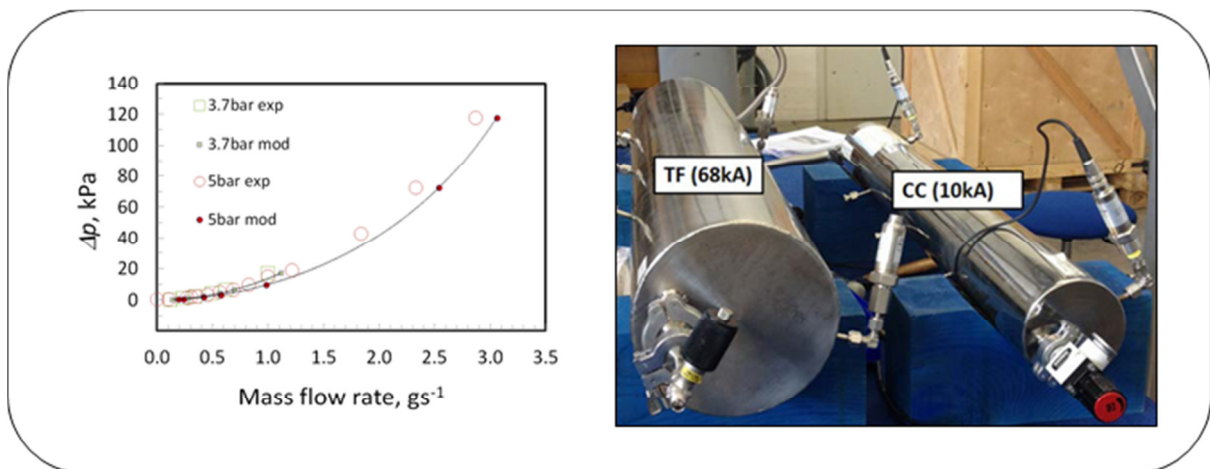


Figure 9: Left: Comparison of model to experimental data obtained on a CC type HX mock-ups with GHe at room temperature, 5 b and 3.7 b inlet pressure. Right: TF and CC-type HX mock-ups during testing at CERN.

17 million degrees of freedom and requires about 3 days to run one steady-state case on a HPC cluster (8-8 sockets). The computer modelling was complemented by an extensive experimental program using mock-ups to characterize the hydraulic behaviour of the HX (further details in section 4.1). Figure 9 shows the computed pressure drop compared with experimental data obtained on a CC-type HX (full length) mock-up. Agreement is at the few-percent level within operational range of flow and pressure.

The HX 3D model was later linked to models of the HTS shunt and the RT terminal to allow full length simulations. This was used to obtain the CERN 3D model data quoted in section 4.

3.2. Other 3D Models

Field Map Model

To calculate the magnetic field and thus determine the amount of HTS needed, a 2D FE electromagnetic model of the leads was developed by IO using TRAPSTM. The distribution of the HTS stacks on a cylindrical surface with the wide face normal to the radius minimizes the perpendicular component of self-field (while increasing the “tangential” component). Since the Bi-2223 critical current, I_c , is more sensitive to magnetic field perpendicular to the broad face than parallel to it, this feature raises the current carrying capability of the lead. In fact the HTS module sees a field that is made up of three parts: 1) the self-field generated by the lead itself, 2)

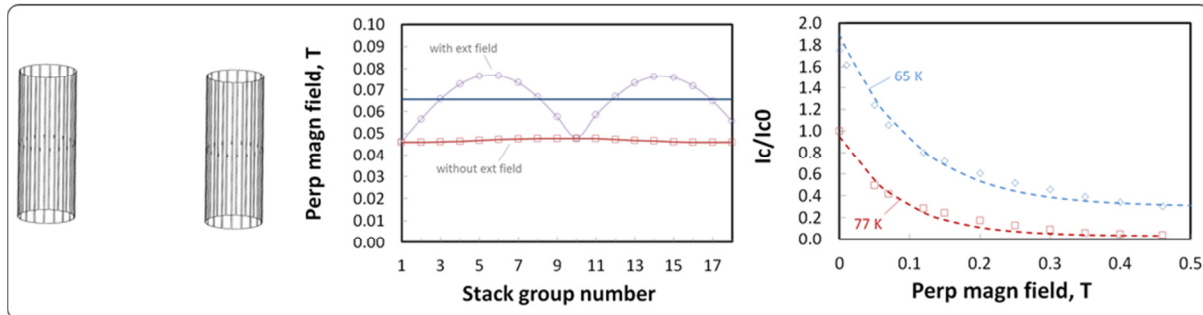


Figure 10: Field map at 68 kA as computed with TRAPS. Left: shunt model; Middle: Perpendicular magnetic field around the stacks (groups of 5) with and without external field; Right: critical current for 65 K calculated with Equ 1 (dashed line) compared to measurements.

the field due to the adjacent lead running opposite current (mounted at ~ 0.5 m distance), and 3) the stray field from the ITER magnet system (at 27 m from the Tokamak center, the stray field is ~ 30 mT, assumed to be vertically oriented here). According to the model the maximum perpendicular component at 68 kA is ~ 80 mT, but varies around the shunt circumference. As shown in Figure 10 the average perpendicular field per stack is ~ 45 mT without and ~ 65 mT with external field. It is well-known (and was further corroborated in the prototype tests [see section 4.3]) that the shunt current carrying capacity correlates with the average value of the perpendicular field (horizontal line in Figure 10), indicating current re-distribution among stacks as the individual I_c is approached. Using a standard fit for the I_c as in Equ 1 [ref 28] – where α and β vary with temperature ($\alpha = 0.3$, $\beta = 1.8$, $B_0 = 0.1$ T for $T = 65$ K, $\alpha = 0.03$, $\beta = 1$, $B_0 = 0.1$ T for $T = 77$ K) – the critical current can be calculated for the given B -field distribution. Based on this (see Figure 10), the average perpendicular field in ITER reduces the critical current by $\sim 50\%$, while the operation at 65 K increases it by a factor 1.8 (with respect to 77 K), such that the HTS module of the TF lead has an operating margin of over ~ 30 kA at 65 K, which translates into a (more relevant) temperature margin of about ~ 15 K.

$$I_c(B) = I_{c0} \left(\alpha + \beta e^{-\frac{B}{B_0}} \right) \quad \text{Equ (1)}$$

Mechanical Model / Supports

In order to optimize the distribution of supports for the busbars in the Cold Terminal Box (CTB), (Figure 11), IO developed an ANSYSTM model of a TF type lead in the feeder including the busbar S-bends and the various supports (RT terminal, flange, mid HX and TB joint). The load cases applied include cool-down, Lorentz-forces due to the Tokamak stray field at 68 kA and seismic loading (vertical acceleration up to 10 g!). The structural element of the current lead is the 3 mm thick stainless steel cover over its full length.

Being attached to the CTB separator plate, the mid-HX support moves down due to the thermal shrinkage of the plate during cool-down and contact is lost with the HX-support (it only plays a role during assembly). The TB-joint support is also pulled down by 0.7 mm, but this roughly corresponds to the natural downwards bending of the lead under its weight and thus contact is maintained. The two leads mounted on either side of the separator plate are also pulled towards each other due the thermal shrinkage of the support arms, causing slight bending. In normal operation bending occurs when the Lorentz-forces are applied, outward or inward depending on the direction of the Tokamak field. Limiting the gap in the TB-joint support to 1 mm, the stress is

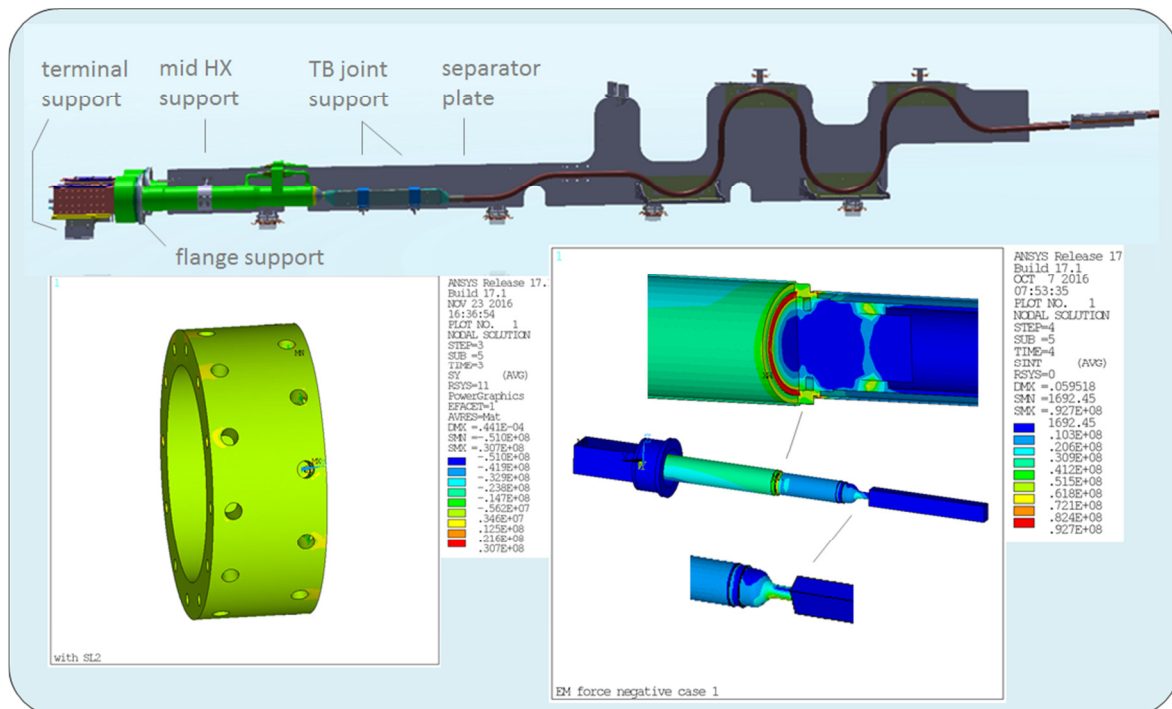


Figure 11: TF-type current lead mechanical model. Top: CAD model of CL in feeder CTB (as modelled in ANSYS); Bottom left: G11 cylinder in-plane stress for full loading including seismic, Bottom right: complete lead Von Mises stress including Lorentz-forces (but without seismic load).

less than ~ 60 MPa in the neck between shunt and TB joint (the “softest” section of the lead). In fact the peak stress (~ 100 MPa in hoop direction) in normal operation appears in the brazing seams between the steel rings and Cu shunt after cool-down due to the small differential thermal shrinkage between the two materials, (see Figure 11). Similar level stresses appear, mostly in the cover of the LTS linker “neck section”, during the (extreme) seismic loading. This stress level is well below the limit, assumed to be $2/3$ of the yield strength of the steel at room temperature (it is mostly far below, providing an additional safety margin). Also note that the internal gas pressure adds only very little to the above. A sub-model of the flange support shows that the stresses are also low (<10 MPa) in the composite even under seismic loading. The G11 flange assembly and cylinder are supported by the solid external support underneath the terminal block.

Integrated Thermal Model

A thermal ANSYSTM model was developed at the Efremov institute in order to verify the thermal behavior of the interface to the air-cooled interface busbar system at the HTS current lead terminal. A number of cases were simulated, including normal operation and fault scenarios. The results of the normal operation cases in the TF type lead, regular DC operation at 68 kA and stand-by operation at zero current are presented in Figure 12. It was found that the temperature of the terminals does not rise above about 40°C when the leads are used at full current. Also, as expected, the terminals stay above freezing temperature in the stand-by case (but require full activation of the terminal heaters). Fault conditions, which were also investigated, include the Loss of Flow Accident (LOFA) and loss of water cooling of the Al busbar system. In the first case the current will be fast discharged at the latest after the LOFA time of ~ 10 mins and the terminal temperature rises only by 5°C . In the second case the current lead terminal is not affected, and the Al busbar is protected from over-heating via its interlock system. For the PF and CC leads the results are similar.

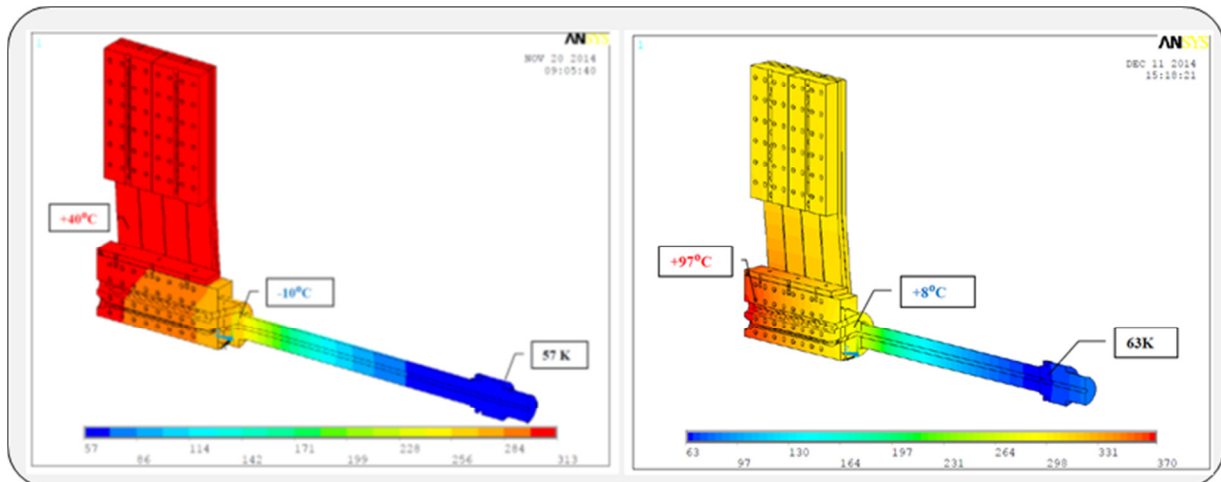


Figure 12: Temperature distribution in current lead terminal region of the 68 kA lead in nominal operation at 68 kA with 4.4 g/s GHe flow (left) and at zero current with 1.2 g/s GHe flow and 3 kW of heating power activated (right).

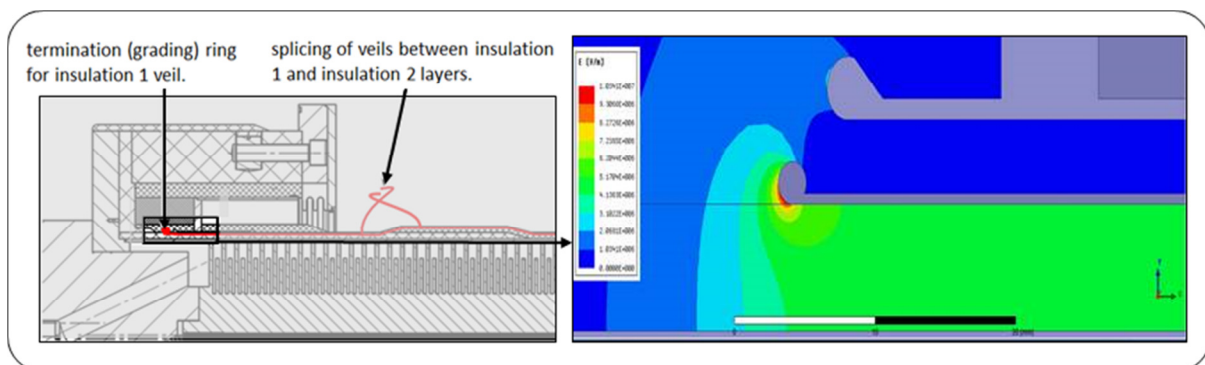


Figure 13: ITER HTS current lead electrostatic model showing the electric field near the ground-shield grading ring (2 mm diameter). The ground-shield and grading ring is shown in red in the sketch of the lead terminal flange area on the left.

Electrostatic Model

While the feeder busbar is fully enclosed in the insulation and its ground shield, the electrical design is more complicated in the current lead, where the conductor emerges from the insulation. Specific issues, especially related to tracking were treated at IO using electrostatic models (Maxwell™). Thanks to these simulations the design of the grading ring at the end of the current lead insulation ground-shield could be finalized, giving a minimum diameter of 4 mm. Figure 13 shows the electric field level peaking at 10 kV/mm for a 2 mm diameter (below the allowable limit but with insufficient safety margin). See section 4 for further discussion on the current lead insulation qualification.

3.3. 1D Models

Transient Model (LOFA and Over-heating Time)

For most purposes and especially for transient cases, current leads can be described with 1D models solving the coupled heat balance equations for the length coordinate x [ref 29]:

$$\frac{d}{dx} \left(\kappa(T) \frac{dT(x)}{dx} \right) + \frac{\rho(T) I^2}{A^2} - \frac{hP}{A} (T(x) - \theta(x)) = 0 \quad \left(\frac{W}{m^3} \right), \quad \text{Equ (2)}$$

where $T(x)$ is the temperature profile along the lead, A the cross-section of the current (I) carrying element, $\kappa(T)$ the thermal conductivity, $\rho(T)$ the electrical resistivity, h the heat transfer coefficient, P the cooled perimeter (heat transfer area divided by length) and $\theta(x)$ the temperature profile in the helium. $\theta(x)$ is obtained by solving the second, coupled equation,

$$hP(T(x) - \theta(x)) = \dot{m} C_{p,He} \frac{d\theta}{dx} \quad \left(\frac{W}{m} \right) \quad \text{Equ (3)}$$

where C_p is the specific heat and \dot{m} the mass flow rate of the helium. First approximation temperature profiles obtained with this approach often match very well the temperature profiles obtained with 3D models. Further refinements are possible through calibration of some of the parameters against experiments and/or 3D models, such as in [ref 30]. In the case of LOFA the GHe flow into the resistive heat exchanger is stopped and Equ (2) reduces approximately to the adiabatic heat balance equation. The temperature evolution of the lead in this case, as computed with the IO model in Matlab™ is shown in (Figure 14). When the HTS quenches, current is “diverted” into the Ag-matrix and the shunt. A simple parallel network model for $\rho(T)$ allows to estimate the overheating time (also Figure 14), i.e. the time it takes the HTS hot spot to reach 200 K at full current after a quench.

HTS Thermal Conduction Model

With dissipation free current transport in the HTS and the absence of He flow, (Equ 2) reduces to Fourier’s law (Equ 4), which can describe the heat conduction across the shunt. Using a parallel conductance model the heat load contributions of the different materials q_i can be estimated from the geometry (cross-section A_i and length L_i) and known material properties (i.e. Figure 4).

$$Q(T_{HTS-top}) = \sum_i q_i = \frac{1}{L} \sum_i A_i \int_{5K}^{T_{HTS-top}} \kappa_i(T) dT \quad (W) \quad \text{Equ (4)}$$

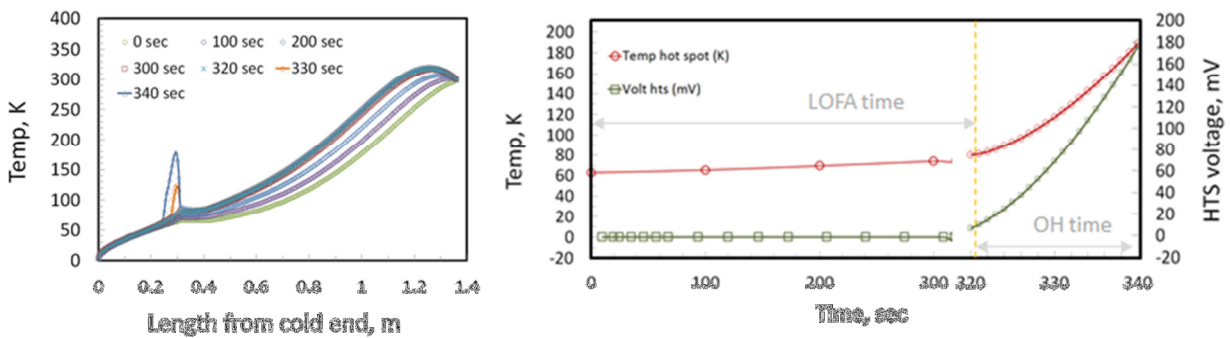


Figure 14: LOFA simulation in a TF-type lead at 68 kA in a 30 mT Tokamak stray field using the adiabatic transient model of the shunt and HX (RT terminal is not modelled). Temperature at the bottom of shunt / top of HX fixed to 4.5 / 300 K. Left: Temperature profiles along the shunt and HX for different times. Right: Evolution of hot spot temperature and shunt voltage during LOFA and the subsequent quench of the HTS.

4. Qualification

The ITER current lead supplier, ASIPP, has chosen two sub-suppliers in the Hefei area - Juneng and Keye - to produce the large leads (TF and PF/CS) and the CC-type leads, respectively. In addition to managing the work, ASIPP procures most materials (and notably the HTS) and some components for issue to the sub-contractors and is responsible for testing of the completed leads. Certain manufacturing procedures were developed firstly by ASIPP and then transferred to the sub-suppliers. The procedures for the three types of leads are therefore similar (there are small differences between the TF/PF and CC types). Specialized sub-contractors have been chosen to supply some specific products and services (HTS material, flange G11 cylinders, electron-beam welding, Ni coating, etc.). The HTS material is supplied in part by SEI (Japan) and Innovia (China). This complete supply chain had to be qualified. For the ITER current leads, phase II of the PA therefore defines two stages, stage 1, the technology mock-ups and stage 2, the prototypes.

As the current lead manufacturing requires several jointing techniques – welding (TIG and electron-beam), high temperature brazing and soldering - the emphasis of the mock-up program was placed on these particular steps. Insulation was also a key area of qualification activities. Finally, however, the acceptance criteria of Table 3 had to be satisfied in the current lead prototypes for the qualification to be successful. The qualification phase allowed all actors (suppliers, DA and IO) to jointly develop the quality assurance for series production. IO contributed with the development of the Manufacturing Data Base (MDB) application, an electronic traveller system to manage the extensive quality documents, with an additional inventory tool for tracking the flow of material and parts across the production (e.g. using bar-code identification). A prototype of this system was successfully used by suppliers, DA and IO during stage 2 of the qualification (prototypes).

Material Qualification (incl. Insulation)

All material is qualified and/or certified according to the applicable codes. The stainless steel is to conform to AISI 316L (level 3.1 certification according to EN 10204). OFE C10200 Cu must conform to standard ASTM B152 with an additional specification for the RRR value (40÷200). Rigorous test schedules apply to the HTS tape. A minimum critical current I_c of 100 A (at 1 $\mu\text{V}/\text{cm}$ according to IEC 61788-3), geometrical parameters (thickness <0.26 mm, width <4.5 mm), thermal conductivity and normal state electrical resistivity, tolerance to bending/tension (<5% I_c degradation after 5 bending cycles to 50 mm radius and 100 load cycles to 75 MPa), matrix chemical composition, HTS filling factor, maximum number of defects were specified. Continuous I_c and geometrical measurements are performed for the entire tape length. The other parameters are measured on some samples taken from each unit length (minimum length specified 100 m). Special requirements are also specified for the thick-walled flange G11 cylinder, which is made by filament winding (alternating with 0 and 10° angle). The R-glass fibers need to comply with ASTM D578, with defined glass (~55%) and void fractions (<2%), minimum laminate shear strength (>30 MPa) and minimum ultimate tensile strength (>300 MPa). The insulation system is qualified according to PA requirements, in particular for void fraction (<2%), minimum laminate shear strength (>50 MPa) and minimum ultimate tensile strength (500 MPa @ 0°, 200 MPa @ 90° to fiber), all after thermal cycling. The qualified insulation materials are all certified off-the-shelf products – Sinoma RW210A-100a[®] R-glass (boron-free, plain weave), Gurit SE84LV[®] / RW210A pre-preg and Dupont Kapton-HN[®].

Welding Qualification

All the TIG welds are qualified according to EN ISO 15614-1:2004 (acceptance levels ISO5817 level B), including the additional requirement of five thermal cycles to liquid nitrogen (LN2) temperature as specified in the PA. Electron-beam welding is discussed further in section 4.1.

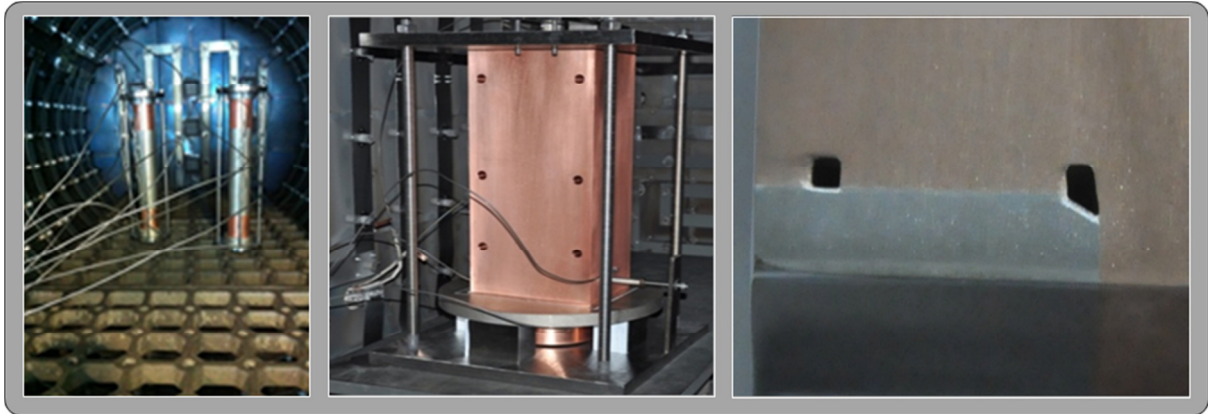


Figure 15: Brazing qualification. Left: CC-type shunt mock-up, Middle: TF type RT terminal mock-up. Right: macro-examination of braze joint. The depleted brazing wire channels are clearly visible.

Brazing Qualification

There are two major brazed subassemblies, HTS shunt and RT terminal, to be qualified according to EN 13134:2000, with the acceptance levels defined according to PA requirements (leak test after 5 thermal shocks). The shunt module mostly consists of a 316L stainless steel cylinder mounted over the OFE Cu end-caps with a 20 mm long overlap (tolerance on gap <math><60 \mu\text{m}</math>) for brazing. In the RT terminal the main brazed joint is between the Cu terminal block and the stainless steel flange. Additional brazed joints are between the terminal and its heat exchanger, and to the instrumentation socket (into which the Fischer plugs get screwed). The braze material (Ag72Cu28) is in the form of wire, assembled into specially machined grooves, and foil. After thorough cleaning the brazing assembly is assembled into a tooling providing axial compression during the brazing at 830°C (the temperature is measured with thermocouples mounted on the pieces) in vacuum. The brazing was qualified on full-scale mock-ups (Figure 15), which were assessed through visual inspection (EN970), leak tested after 5 thermal shocks and destructively evaluated (metallography and tensile test according to ASME section IX). Imperfections were within the limits set by ISO 13919-1 level B. In the tensile test, failure occurred as expected (at ~180 MPa) in the copper, not in the braze joint.

Soldering Qualification

No specific codes are available for low-temperature soldering, so the processes were qualified by mock-ups (see section 4.1 for further details). The acceptance levels followed PA requirements (visual examination of bonding after 5 thermal shocks, electrical test at operating temperature).

Bellows Qualification

Bellows, made from welded sheet and hydro-formed, were designed according to the EJMA code (9th edition) and qualified according to the PA requirements (leak test after displacement fatigue test and multiple pressure cycles).

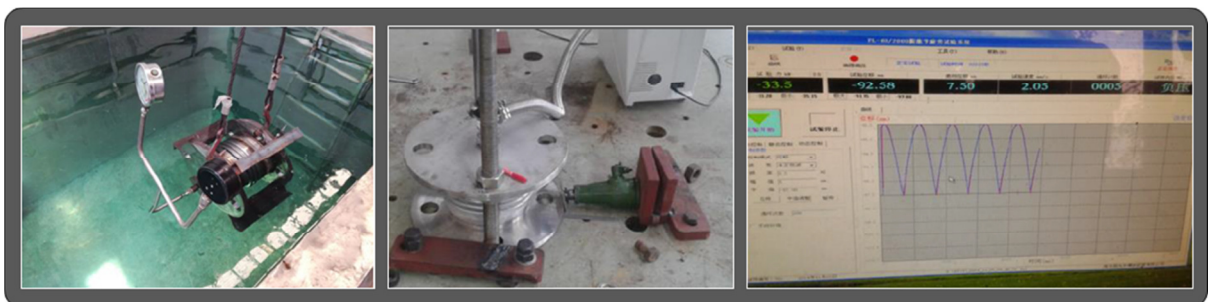


Figure 16: Bellows qualification, Left: leak testing in water pool, middle and right: fatigue testing.

Twin-Box joint Qualification

With hundreds of box-type joints inside the ITER feeder system, the box joints were separately qualified in the framework of the feeder qualification. Further details of this qualification are reported in [ref 24]. However, although the box joint at the cold end of the current leads uses the qualified feeder design, there is one notable difference: the TF and PF type current leads use eutectic Pb-Sn solder instead of In for bonding the cable to the Cu sole. This is because the In in the joint box would melt during the soldering of the stacks to the shunt and LTS linker component in the vacuum furnace. As will be discussed in section 4.1, it was shown in the TF-type LTS linker mock-up, that (as expected) good bonding can be achieved with the Pb-Sn process. The TB joints of the prototype current leads performed well within the ITER specification, i.e. DC resistances below 2 n Ω / 5 n Ω for the TF / CC types and the expected pressure drops (~10 mb / single TF box at ~5g/s SHe flow or ~80 mb for a twin-box at 10.5 g/s. the nominal SHe flow in the TF feeder busbar, see Table 6). A major related effort was the development of suitable 316L steel – OFE Cu clad plates used for machining of the joint box [ref 31]. It was found that the joint clad plate must be examined thoroughly to validate good bonding at the Cu/steel interface.

4.1. Mock-ups

Mock-ups were specified in the PA agreement (phase II, stage 1) as a pre-requisite for the start of prototyping [ref 32]. The experience gained and results obtained in the campaign are presented. Further discussion of mock-ups can be found in [ref 33] and [ref 34].

HTS Shunt Mock-ups

The stacks are manufactured by alternating n pre-cut tapes and $n-1$ solder foils into a mould, where $n= 8/7$ SEI tapes⁵ for each TF/PF stack, and 5 Innovia tapes for each CC stack. The mould is then heated in vacuum to 240-250°C for 15 mins (as measured with Pt sensors) to ensure the melting of the Sn-3.8Ag-0.7Cu solder (melting point 217°C), whilst pressure is applied to ensure compaction. After cool-down and extraction from the furnace the stacks are placed in a go/no-go gauge to ensure the maximum width of 4.5 mm is respected. They are also weighed to determine the solder loss ratio (typically ~60%). After critical current testing, 5 mm is trimmed from each end, to remove areas which are potentially damaged by the pressure contacts in the critical current test rig.

To qualify the stack-shunt soldering joints a 1/30 sample of a TF type shunt module was manufactured and tested. It consisted of three Bi-2223 HTS stacks soldered to a Cu-steel brazed plate, with a LTS sub-cable soldered into it (as described for the LTS linker mock-up). After dipping into LN₂, 1 kA current was applied. The joint resistances of joints A and B were 5.2 n Ω



Figure 17: TF shunt soldering mock-up.

⁵ The reduction of the number of tapes per stack is possible because of the higher than specified critical current of the SEI tapes (typically > 170 A vs 100 A specified). The same temperature margin (or more) can thus be obtained with a smaller stack. The resulting (small) reduction in over-heating time was calculated to be still within specification (with the model discussed in section 3.3). The reduced number of tapes decreases the heat conduction across the shunt, thus improving this aspect of the design.

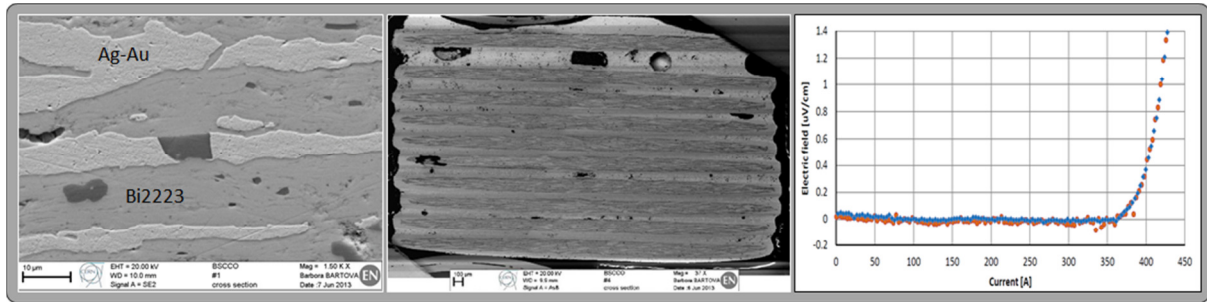


Figure 18: Left: micrograph of Innovia Bi-2223 tape, Middle: stack made by CERN from Innovia tape, Right: critical current measurement of two 5-stacks (CC-type) in self field @ 77 K.

and 3.0 nΩ. In a real TF lead there are 30 such joints connected in parallel, thus the extrapolated resistance of a full size joint would be 0.1~0.16 nΩ, well within the required 1 nΩ. Besides measurement of the joint resistance a major goal was to determine the amount of solder to place between the layers of tapes (the finally chosen foil thickness is 0.05 mm).

Tape and stack samples were also investigated at CERN and made into stack samples (Figure 18). Porosity found in the Ag-Au matrix of earlier tapes from Innovia were not found in subsequent samples. No evidence was found of “bubbling” observed in some early stacks for the LHC leads.

LTS Linker Mock-ups

The current lead sub-components requiring the most complex assembly is the low temperature end of the lead, which includes the joint box and the LTS section with several soldered electrical contacts. Figure 19 shows the TF type linker mock-up made by Juneng as example. A similar mock-up was also made by Keye for the CC-type.

The LTS linker manufacturing starts from a ~1 m long piece of ITER magnet feeder busbar (main bus in the case of TF, PF and CS leads and the corrector bus for the CC lead), stripped of its jacket at both ends and prepared for pre-tinning. This requires first the removal of the micron-thin Ni coating on the LTS strands. At the shunt end, the cable is dis-assembled into the 30 (12 in the CC lead) stage 3 sub-cables. The Ni is removed chemically using OY54. The other end, which goes inside the joint box, the Ni on the outer surface of the cable is removed by reverse plating (i.e. the Ni is electro-chemically replaced by Ag). Following chemical cleaning, passivation and thorough rinsing, both ends are pre-tinned. First, on the shunt side end, the sub-cables are coated with Sn-3.8Ag-0.7Cu (melting point 217°C) solder by painting with non-corrosive flux and dipping in a solder bath. In the case of the CC leads, the 12 sub-cables are disassembled and each strand is tinned separately, followed by rebuilding of the sub-cables. This is followed by a multi-stage moulding process, in which the pre-tinned sub-cable is subsequently pressed (while heated) into the desired diameter to fit into the holes machined into the shunt Cu-cone (Figure 20). The most critical step is the soldering process between these sub-cables and the



Figure 19: TF-type LTS linker mock-up (before destructive testing).

Cu-cone during the joining of the shunt and LTS linker sub-components. A specification for the electrical resistance must be met, requiring 100% wetting by solder of the bare strands, a tight fit between sub-cable and hole and complete filling of voids with solder. The calibrated holes in the Cu terminal are also pre-tinned with Sn-Ag solder to facilitate the reflow soldering that is performed in vacuum at 240°C for 10 min. Using small scale mock-ups, such as the one discussed before, a special method was developed, which consists of first heating the assembly in vacuum until the solder has melted, followed by repeated pressurizing of the volume with N₂ gas and possibly moving up and down the sub-cables inside the blind holes to ensure all trapped air is released (Figure 21). This method has been tested and found to produce very compact solder joints with a resistance of a few nΩ per sub-cable, thus satisfying the requirement of less than 1 nΩ for the entire joint (made of 30 sub-cables). After reverse plating, the other (joint box side) end is assembled into the joint-box together with a 0.3 mm Sn63Pb37 solder foil to improve the electrical contact to the Cu-sole. Microscopic, x-ray and mechanical examination of the mock-up joints demonstrated good bonding (Figure 22). After the joint cover is welded on under the press, the entire shunt and LTS linker module is heated in the vacuum furnace to 213°C to melt and diffuse the solder along the cable/Cu-sole interface (solder melting point 183°C). The foil should not have melted during the joint box welding, however. Therefore an intermittent welding pattern, together with continuous Ar flow inside, keep the peak temperature in the Cu sole to less than 70°C, as recorded on the mock-up. Also, in order to avoid degrading the superconducting properties of the NbTi LTS, its maximum temperature in any of the multiple heating steps during the LTS linker manufacturing must remain below 250°C and the time spent at greater than 200°C measured and recorded (total should be less than 3 hours). After 5 thermal cycles to LN₂ temperature, the LTS linker mock-up was pressurized to 3 MPa (the test pressure for the SHE circuits in the ITER feeders) with GHe and leak checked to the level of 10⁻⁹ Pa·m³/s, as for any feeder component.



Figure 20: Preparing the sub-cables (TF-type): Left: chemical Ni removal, Middle: pre-tinning, Right: soldering into the shunt blind holes.

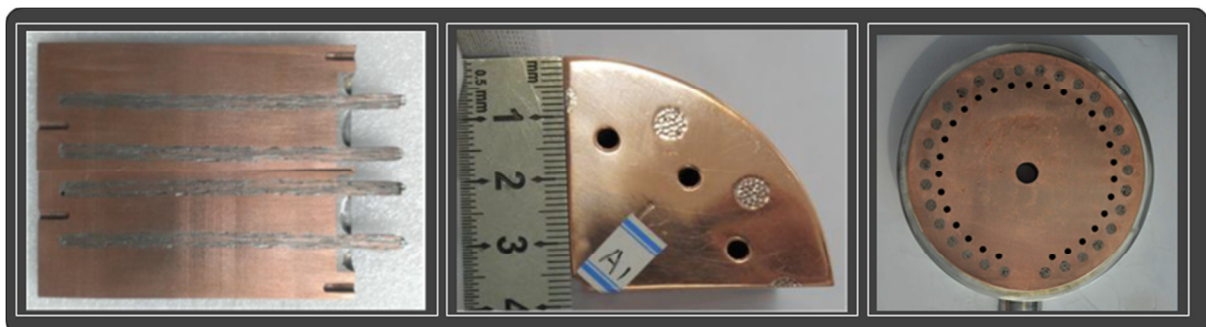


Figure 21: Destructive investigation of the sub-cable to shunt solder joint. Left: soldering trials in sub-scale mock-up, Middle: Macro-examination CC-type LTS linker mock-up, Right: Cut through the TF-type LTS linker mock-up.

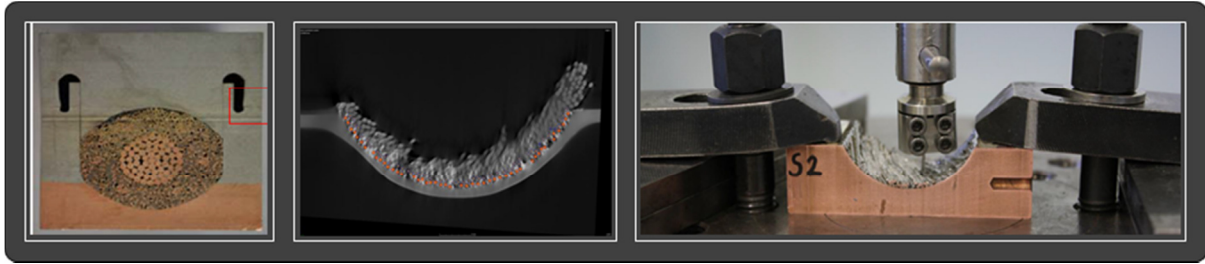


Figure 22: Destructive examination of the LTS linker TB-joint. Left: metallographic cut, Middle: X-ray tomography for solder filling investigation (performed by CERN), Right: strand peel-off tests for bonding strength evaluation (performed by CERN).

HX Mock-ups

Following an early mock-up made at CERN to demonstrate the general feasibility and manufacturing technology, full size HX mock-ups of the TF and CC types were manufactured at Juneng and Keye to verify if the tight H7g6 manufacturing tolerances could be achieved between the core and honed tube (Figure 23). First trials of core machining by lathe revealed that the tolerances could not be met. The manufacturing time was also too long (at least for the TF type). Automatic multi-axis CNC machining reduced this to less than 1 week. Keye decided to continue with the lathe approach, but the manufacturing tolerances had to be relaxed. As verified by FE modelling sagging under its own weight causes a straightness deviation of $\sim 200\ \mu\text{m}$ when mounted on the lathe⁶. The key QC on the HX core is the dimensional measurement in the Coordinate Measurement Machine (CMM). As the fins are clipped on alternating sides, the fin OD cannot be measured over the full circumference. Different options were studied, but finally it was decided to measure the OD over 20 points distributed over half the fin circumference. The calibrated ball-sensor has to move to alternating sides of the HX core going from fin to fin to avoid the clipped sections. This has proven to be sufficient for precisely measuring the straightness (specified to be within 0.07 mm for the TF-type lead) and OD (within 0.03 mm on 188 mm for the TF type lead).

The tight specifications for the tube sliding over the HX core (the so-called HX cover) can only be obtained by honing. A feeler gauge mounted on a special tooling is used to measure the dimensions. Corrections for the 3D axis mismatch between the sliding measurement system and the tube need to be taken into account in the data reduction. Temperature control during honing and measurement is critical. A full length go/no-go gauge is used for a final acceptance test of the honed tube.



Figure 23: HX mock-up manufacturing: From left to right: HX core machining in a CNC, honed tube dimensional check with a feeler gauge, HX core dimensional check in the CMM, HX Assembly.

⁶ The reason is the low stiffness of its design (the CC core is further “weakened” by the 10 mm central channel for the instrumentation wires). As discussed below, for the same reason it is difficult to machine it to tight tolerances, the “soft” HX core is easier to insert into the honed tube as it more readily adapts to its shape.

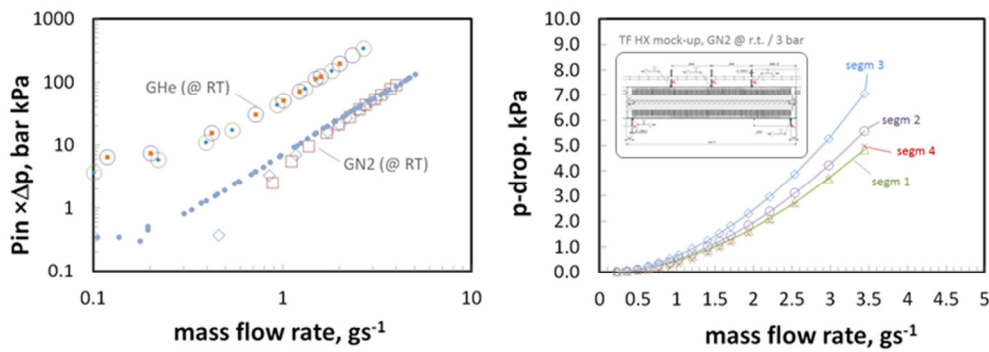


Figure 24: Pressure drop tests in TF HX mock-ups performed in GN₂ and GHe at room temperature. Left: ASIPP data (full symbols), CERN data (open symbols), Right: GN₂ measurement in TF HX mock-up with distributed differential p-gages, covering each a quarter of the length, note that the gage of segment 4 was less accurate (50 kPa range instead of 10 kPa), possibly explaining the unexpected result.

Although first demonstrated by CERN with a special assembly mock-up, the assembly of the honed tube over the HX core was found to be difficult and some early trials resulted in failure. The strategy that was finally adopted consists of heating the honed tube to 100°C, causing its diameter to increase by ~0.3 mm, and then manually slide it over the vertically pre-assembled lead. The idea of using a sliding assembly tooling was quickly abandoned as it required very precise tooling dimensions, even more precise than the HX components themselves. Special tooling is used to hold the lead upright and set up the honed tube above the lead before the operation.

The HX mock-ups were then submitted to a series of pressure drop tests with GN₂ (nitrogen gas) and GHe at room temperature to establish a set of reference data for the future prototyping and series manufacturing. Due to their importance the measurements were performed at ASIPP and then repeated at CERN (the HX mock-ups can be seen while being tested at CERN in Figure 9). In accordance with the (Darcy-Weissbach) friction factor model, the pressure drop data multiplied by the inlet pressure for one type of test gas all fall on one curve, i.e. for a given mass-flow rate the pressure drop increases at lower inlet pressure (Figure 24) as both depend on the gas density ($p \sim \text{dens}$, $\Delta p \sim \text{dens}^{-1}$). A small difference remains between the CC and TF data, hinting at a factor ~2 difference in friction factor between the two designs (CC data are not shown in the figure), possibly related to the size of the cuts at the ends of the fins. Both mock-ups, but in particular the CC-type, show a transition from turbulent to laminar flow at the lower end of the operational flow-rates (which complicated the measurements). The comparison of the experimental data to the model helped the calibration of the model (see Figure 9). This and other aspects of these data are discussed in [ref 35]. Figure 24 also shows a special measurement performed on the TF HX mock-up in which capillaries were inserted along the HX to measure the pressure drop along four equally long sections. As expected the pressure drops of the four sections agree, except for a slight increase from upstream to downstream resulting from the inlet pressure (into the specific segment), which is smaller for each segment as a result of the pressure drop in the previous segment(s). Finally X-ray tomography was used at CERN to verify that there were no bent fins or other defects in the HX honed tube assembly, which could not be detected by the pressure drop method (none was found).

Electron Beam Welding Mock-up

Electron-Beam Welding (EBW) was qualified according to EN ISO 15614-11:2004⁷. A special mock-up was made to develop the welding procedure. In addition to the ISO 13919-1 level B acceptance requirement, internal requirements were defined in the PA, including vacuum leak

⁷ Note: this code applies for steel and not Cu. As there are no special codes available for Cu, this code was adapted to Cu and applied.



Figure 25: EBW mock-up results. Left: TF-type ebw mock-up, Middle: samples for micrographic examination of weld, Right: tensile strength measurements of weld samples.

tests after thermal shocks and the evaluation of the length of the heat affected zone. Local defects of 2 mm were found in the metallographic testing of the TF-type mock-up, thus the delivered welding quality level was ISO 13919 C. In the CC-type mock-up, however, level B was reached. It was therefore decided to accept the non-conformance in the TF type EBW mock-up. Also the peak temperature reached at the position of the HTS stacks, 132°C / 171°C in the TF / CC mock-up, was, for the CC case, at the limit of the acceptable (just 12°C under the solder melting point), but nevertheless found to be acceptable as the related Cu mass in the real current lead is much larger than in the mock-up and thus the expected temperatures lower. Tensile samples failed outside the weld-seam at > 180 MPa (the failure limit in Cu), see Figure 25.

Insulation Mock-up

As noted above the ITER magnet feeder PA defines stringent qualification requirements for the insulation system. To these are added particular requirements for the resin curing temperature (see section 2.5) and for the maximum boron content (zero, to prevent nuclear activation). The test requirements also include partial discharge and Paschen testing. The development of a 30 kV class, combined polyimide / impregnated glass fiber system required a significant R&D (also because the experience for such an insulation system is limited in the low temperature community). The IO (via the Rockwood company) and ASIPP efforts are discussed in further detail in [ref 36] and [ref 37]. A key factor of the insulation development as found in this work is the compression during curing. The 30 kV insulation system finally developed for the current leads uses 5-6 bar pressure produced in an autoclave to compress the 9 half-overlapped layers of “GK” wrap made of compounded 0.2 mm thick, 25 mm wide pre-preg glass tapes and Kapton HN polyimide tapes with 50 µm thickness⁸. The insulation is built in three separate autoclave curing stages to improve compaction. The particular geometry of the current lead in the conical section and at the perpendicular pipe “branch-offs”, requires a different layering pattern – along, not around the pipes – and full overlapping to satisfy the tracking length requirements for the insulation (175 mm in TF and PF type, 30 mm in CC type). The partial discharge levels found in

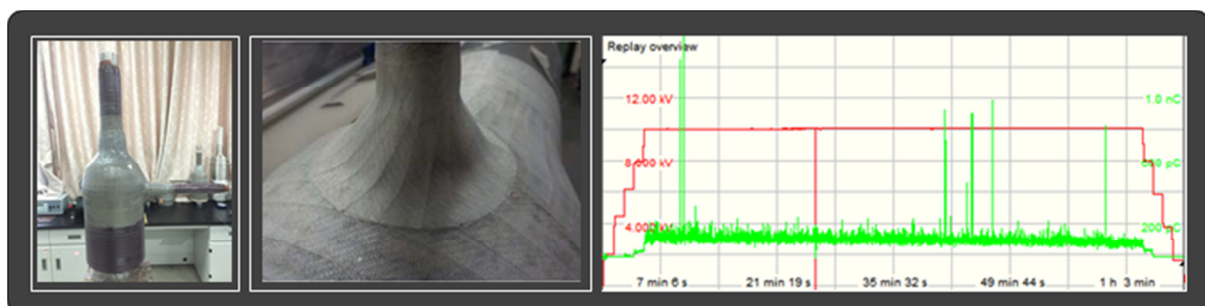


Figure 26: Current lead insulation mock-up. Left: ASIPP mock-up, Middle: Rockwood mock-up, Right: PD test of ASIPP mock-up for 60000 cycles at 10 kV rms.

⁸ The part of the current lead insulation that is outside the cryostat (and thus not in a Paschen atmosphere), i.e. the flange assembly, is not made in the autoclave but with Si-rubber wraps to apply the radial pressure.

the mock-up tests in Figure 26 are consistent with those of small, flat insulation samples for which the void fraction was measured to be within specification.

Insulated Heaters for the Room Temperature Terminals

If the electrical heaters are at the high potential of the current lead terminals, their power supplies must be isolated to ground – such isolation transformers are large and expensive and since they cannot be placed near the feeder terminals due to radiation, magnetic field and space constraints, they contribute to spreading the HV (which in turn adds to the bill as it requires expensive HV cables). An interesting alternative (also used in the KSTAR Tokamak, albeit at lower voltage) is the use of insulated heaters, i.e. to insert the cartridges into insulating sleeves. Ceramic cannot be used due to its fragility, nor Teflon due to its sensitivity to nuclear radiation. The material finally considered is sintered polyimide (PEEK). It has a reasonable 0.4 W/m-K thermal conductivity, >20 kV/mm electric breakdown field, 118 MPa tensile strength and even good machining properties. Qualification experiments were carried out in IO in a thermal mock-up mimicking the current lead terminal. For thermal test, the full power (500W) was applied to check the heat transfer characteristics and maximum heater temperature (<100 K). It passed the electrical tests, 60 kVDC and 20 kVAC, at 200°C. It is expected, however, that regular replacements of the heater sleeves during the ITER life-cycle may be needed. Alternatively (should the replacement frequency turn out to be high) the water cooling pad could be used in conjunction with a water heating system to heat the terminal. The efficiency of such a system could be improved significantly by re-circulating the water or in combination with a counter-flow heat exchanger to pre-heat the incoming water. Such a heater would obviously be placed on the low voltage side of the flexible EPDM water hoses used to galvanically isolate the water pad from the cooling water distribution piping.

Room Temperature Insulating Breaks

The ITER superconducting magnets built from CIC conductors require thousands of insulating breaks to insulate the cryo-lines supplying the magnets from the coil potential. In ITER (as well as most other fusion Tokamaks) these insulating breaks are made by embedding metallic electrodes in a glass-fiber composite. Since the HTS current leads discharge the GHe at room temperature, the GHe exhaust lines need to be isolated with such insulating breaks operating at room temperature and possibly down to atmospheric pressure. Due to its low density helium gas has very poor dielectric strength in these conditions (approximately 12 times less than air), much poorer than at high pressure and low temperature such as in the cryogenic supply lines of the coils. Designs for the Room Temperature Insulating Breaks (RTIB) therefore needed to be developed especially for the HTS current leads. The conceptual approach consisted in lengthening the electrode to electrode distance and increasing the electrode diameter such as to reduce the electric field anywhere inside the GHe channel to below 300 V/mm at the design voltage (this limitation does not exist in a “cold” IB). Since these design parameters cannot be increased without drawbacks, in particular for the stresses inside the composite, the design margin (approximately a 50% margin with respect to the worst case fault voltage rather than the “usual” >100%) is smaller in the RTIBs. Further discussion on this development and in particular on the HV tests of some of the prototypes can be found in [ref 38]. Also note that the RTIBs need a ground-shield to reduce local field enhancement effects due to sharp corners in the grounded structures nearby, but this cannot be located too close to the surface of the IB because it also affects the peak electric field inside – the closer it is, the more it enhances the electric field inside the GHe channel. For the large RTIBs (TF,PF) it was found that the shield must be 10 cm away from the surface to limit its impact on the electric field in the gas channel.

4.2. Prototype Manufacture

The manufacturing of the prototypes implemented the ITER approved designs as described in section 2, which included improvements borne from the technological mock-up program discussed in section 3. The following lists the most important changes:

- ✓ instrumentation end-dome machined from one piece to avoid complicated welds,
- ✓ sub-cable “positioner” Lorentz-force support in LTS linker removed as unnecessary,
- ✓ changed design of cooling pipe to transition and bottom ring welds from “internal” to a standard butt weld, as it proved more difficult to perform the internal welds,
- ✓ increased blind hole diameter in shunt to allow for larger sub-cable diameter as typically obtained after moulding in mock-ups,
- ✓ relaxed straightness requirements for HX core (slightly for TF/PF, more for CC),
- ✓ strengthened the shunt bottom backing plate design and weld (to better resist the 3 MPa pressure differential),
- ✓ increased the depth of the room temperature terminal heater holes to 0.5 m,
- ✓ increased the weld depth for weld between conical cover and bottom shunt ring to ensure consistent 3 mm cover thickness over the entire length (cover shape also changed),
- ✓ changed instrumentation wiring from AWG 24 to AWG 28 to better fit the wires into the central instrumentation wire channel,
- ✓ changed shunt Pt100 sensor connection plate into a two-plate design (so that the printed circuit board can be flat as preferred by the pcb manufacturer),
- ✓ increased the weld and focusing lens currents for the TF/PF eb-welds,



Figure 27: Prototype manufacturing. a-b): sub-cable preparation and soldering, c): LTS linker completed, d) soldering LTS linker into shunt, e) terminal brazing preparation, f) stack on shunt assembly, g) stack to shunt soldering, h) TB joint assembly i) TB joint pressure welding, j) HX geometrical testing, k) electron beam welding, l) honed tube assembly, m) mounting of temperature sensors, n) embedded ring glass wrap, o) bellows welding, p-q) main insulation, r) flange cylinder glass overwrap.

- ✓ changed the brazing configuration from horizontal to vertical (only for CC as shown in Figure 15, as in the TF/PF cases the configuration was already vertical in the original qualification) following a failed shunt brazing when the pre-compression fixture got “caught” in the furnace grid during cool-down,
- ✓ finalized the insulation design: - switching from nine to seven GK layers (for CC only) - removed complex G11 form pieces (green putty instead) - added grading ring for ground-layer termination - added corrugated filler to increase tracking length of embedded ring assembly - use of semi-conductive tape to smooth sharp edges in the transition and bottom ring areas - added corrugated half-shells around the PF flange cylinder to increase tracking length;

Some snapshots of the prototype manufacturing are given in Figure 27. Manufacture of the TF and PF current leads went without major incident. Most noteworthy among the minor incidents were the weld-through of a TF instrumentation vacuum valve (later cut and replaced), a failed brazing of the same instrumentation vacuum pumping pipe on a PF prototype terminal (2) and a TF shunt (2) to stack soldering operation in which the cold end of the stacks was not properly vacuum soldered to the shunt. The failed brazing was cut out and re-brazed with a lower melting point brazing alloy. In the latter case the stacks were carefully removed while heating, the shunt cleaned and re-soldered with an improved procedure to ensure a more uniform temperature distribution across the shunt (in vacuum furnace instead of with band heaters). This improved procedure will also be used in the series leads. Some defects found after Ag coating of one of the PF lead shunts was traced back to insufficient cleaning. During manufacture the lead engineers proposed to mount the HX honed tube before instrumenting the shunt to avoid possible damage to the instrumentation. This procedural change was of course promptly implemented. Similarly manufacture went smoothly for the CC prototypes. Only two incidents are worth noting – the shunt brazing had to be re-qualified for vertical orientation following a failed brazing (as discussed before), and one of the shunt steel sections developed a leak (without impact on function) after brazing, presumably due to imperfections in the steel plate from which it was machined (some of the steel used in the prototypes was not fully qualified to the required standards as will be the norm for the series manufacturing). This non-conformity was accepted since the prototype leads *will not* be used in the ITER machine. As the insulation design was evolving during the prototyping effort, some leads were insulated at least twice, demonstrating that it is possible to remove the cured insulation completely from a lead (process essentially done by hand with chisels and grinders), a useful experience for the future. The finally produced prototypes (one of each) are shown in Figure 28. Obviously the prototypes were also instrumented with additional sensors, in particular in the HTS region (temperature sensors and voltage taps).



Figure 28: PF prototype lead, Background: TF prototype lead (left), CC prototype lead (right).

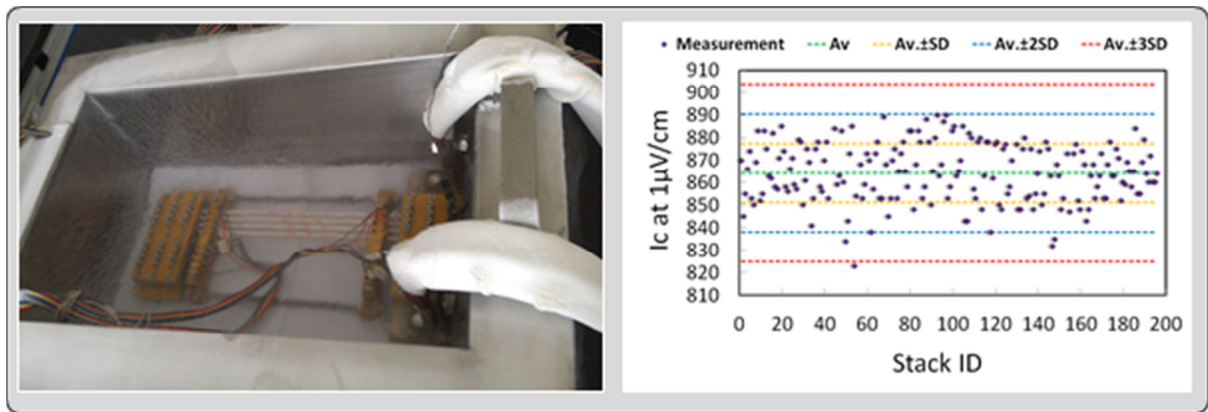


Figure 29: Stack I_c test rig (left) and stack I_c test results for the TF prototypes.

HTS Stacks

For the manufacture of the TF-PF / CC prototypes approximately 2.3 km (9 unit lengths) / 560 m (one unit length) of HTS tape were procured from SEI / Innovia. The production of the HTS tapes and soldering into stacks are key processes, which were thoroughly qualified through mock-ups and then the prototypes. As previously discussed the number of tapes per stack was reduced in the TF (8) and PF (7) leads, as the SEI tape consistently gave a tape I_c greater than 180 A. ~200 / 200 / 80 stacks of the TF / PF / CC type were vacuum soldered in a mould (two at a time) and tested for the prototypes. Figure 29 shows the results of the I_c testing of the different stacks together with the test rig (which can test up to 8 stacks per run). The specified stack I_c of the TF/PF/CC type stacks of 750/620/350 A at 77 K (in self field) were easily reached. To illustrate the use of the production database (MDB) the measured and recorded solder loss ratio for the PF and TF prototype stacks is shown in Figure 29. The 3- σ SPC limits are respected, indicating that the manufacturing process is well under control.

4.3. Prototype Testing

A pair of each type of ITER HTS current lead was tested as the final step of the qualification process. The tests were conducted at different stages of manufacturing. First the leads were cold tested under nominal current and thermally cycled without insulation. Then, the insulation was added and the leads were electrically tested, including in Paschen conditions. Finally an ITER feeder systems test was conducted in which the current leads were assembled into a prototype feeder⁹, including jointing to the busbar system, then thermally and mechanically cycled and HV tested again. The purpose of all these tests was to verify compliance with the qualification criteria (Table 3). A pre-defined test plan was executed, which included tests in nominal conditions (including the LOFA fault case), and tests at different currents and for different cryo-conditions at the HX inlet. Finally pulsed mode tests were also conducted. The experimental results were compared to the predictions from the models discussed in section 3. More details on CC and PF prototype manufacture and testing are discussed in [ref 39, ref 40] and [ref 41]. Here we focus on the TF prototype test results, as they are not reported elsewhere.

Test Facility

The tests were conducted in a new ASIPP test facility including a 900 W @ 4.5 K He plant and a 80 kA power supply system as described in [ref 42]. It also includes a control and interlock system supplied by IO. Figure 30 shows the layout for the HTS-current lead test. Figure 31 shows

⁹ This so-called ‘‘S-bend mock-up’’ activity is a systems test at the feeder level and thus formally beyond the scope of the HTS lead qualification, so it is not discussed in detail here (see section 5.2 for some information).

some pictures of the test facility. Two current leads were mounted in series inside a prototype of the ITER Coil Terminal Box (CTB), shorted by a removable superconducting U-bend with clamped TB joints. The leads were fully instrumented with voltage taps for continuous quench detection and measurement of the different joint resistances and with temperature sensors in key locations. The 50 K and 5 K hydraulic circuits were also fully instrumented with pressure gages and temperature sensors at the inlet and outlet as well as flow meters at the outlet. The two HX were supplied in parallel (and thus independently) with 50 K GHe with the flow being regulated with a valve downstream of the 300 K GHe exhaust of each lead. At the 5 K ends the leads were supplied in series with SHE, with the SHE entering through the TB joint of one lead, then flowing through the CIC-type U-bend and exiting after the LTS linker of the second lead. The 5 K GHe could be heated to room temperature in a large heat exchanger downstream of the CTB, to allow a precise flow measurement with a flow-controller. A cold Venturi tube was also installed in case the warming of the gas over-burdened the liquefier (which sometimes happened). In order to improve the precision of flow measurement at room temperature the 5 K flow was only warmed up to RT for the zero-current heat load measurements. Current was supplied from a large power supply system built specifically for ITER component testing (the “DC platform” for testing ITER power supply components provided by the PRC). As will be done for the final ITER installation, large water-cooled Al busbars transfer the currents from the power supply building to the HTS current lead test-station, where (IO supplied) air-cooled flexibles are used to connect them to the current lead terminals.

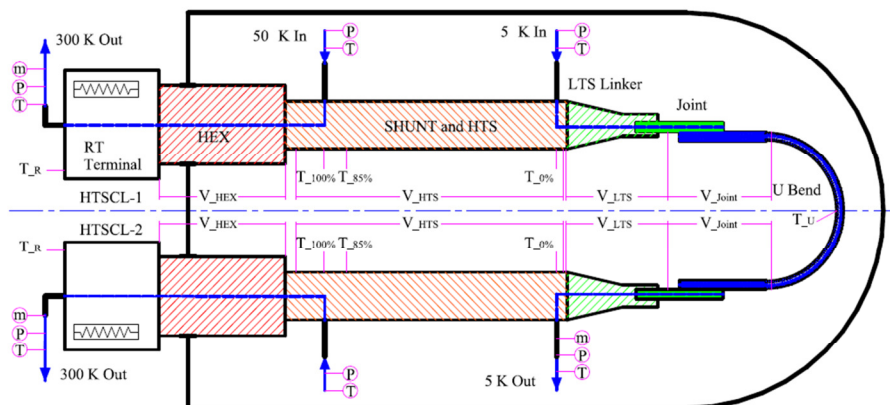


Figure 30: ITER HTS-CL test schematic.



Figure 31: PF HTS-CL prototypes inserted into the test cryostat.

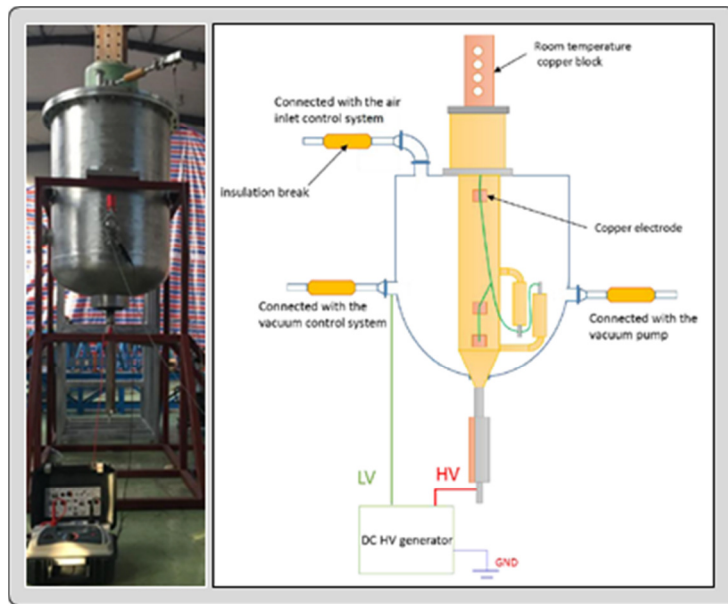


Figure 32: Paschen-testing of the HTS leads. Left: Paschen test vessel. Right: test schematic.

For convenience, HV-testing, in particular Paschen testing, was performed in a separate test system, independent of the cold tests. The special Paschen test vessel allows the non-insulated TB joint section of the lead to remain outside the Paschen atmosphere (Figure 32). The outer ground screen of the current lead insulation is connected to the test vessel. The HV is applied to the naked joint (or RT terminal). During testing the 5 and 50 K outlet/inlet have welded covers such that the hydraulic circuits and in particular the inside of the Insulating Breaks (IB) can be filled with air at ambient pressure, to prevent Paschen breakdown inside the IBs. The air pressure in the test vessel is varied from ambient to 1 Pa, and HV is applied in steps up to the levels given in Table 3. The lead sensors are protected with a “shorting” connector inserted into the instrumentation plugs on the RT terminals. The vessel is equipped with viewing windows and cameras to observe arcing.

Test Matrix

The items in the test matrix for the prototype qualification in Figure 33 correspond to the acceptance parameters defined in Table 3. Three thermal cycles were required to check for degradation during cool-down /warm-up cycles. Most of the key tests were conducted during the first thermal cycle. The leads were operated in steady state (with and without current) at the design current to compare the behaviour to the design expectations. Steady state operation is achieved when flow and temperatures are stable for at least one hour: the flow-rate and voltage in the HX are key parameters to be measured in this condition. This test was followed by a LOFA test in which the 50 K supply to the HX was stopped and under continued DC current the evolution of temperature in the HTS and HX was observed. Following the quench the so-called overheating time was recorded, i.e. the time it takes for the shunt hot spot to reach 200 K (for this test the interlock settings of the control system had to be modified). Steady state and LOFA tests were repeated for each thermal cycle to detect possible degradation of the lead performance. During the first thermal cycles three additional test blocks were performed – the so-called “over-cooling” study, the “over- and under-current” study and the study of pulsed operation. During the over-cooling study the temperature and pressure of the 50 K GHe supply to the HX was varied. During over/under-current runs the operational characteristics of the leads were studied for different DC currents, and compared with simulations. In the pulsed operation several HX operational control patterns were tested with current pulse cycle foreseen for the operation of the PF and CC type leads in ITER. Tests were also conducted to measure the resistance of the various splices (Cu to HTS, HTS to LTS, TB-joint) and to measure the heat load to the 5 K end. Finally

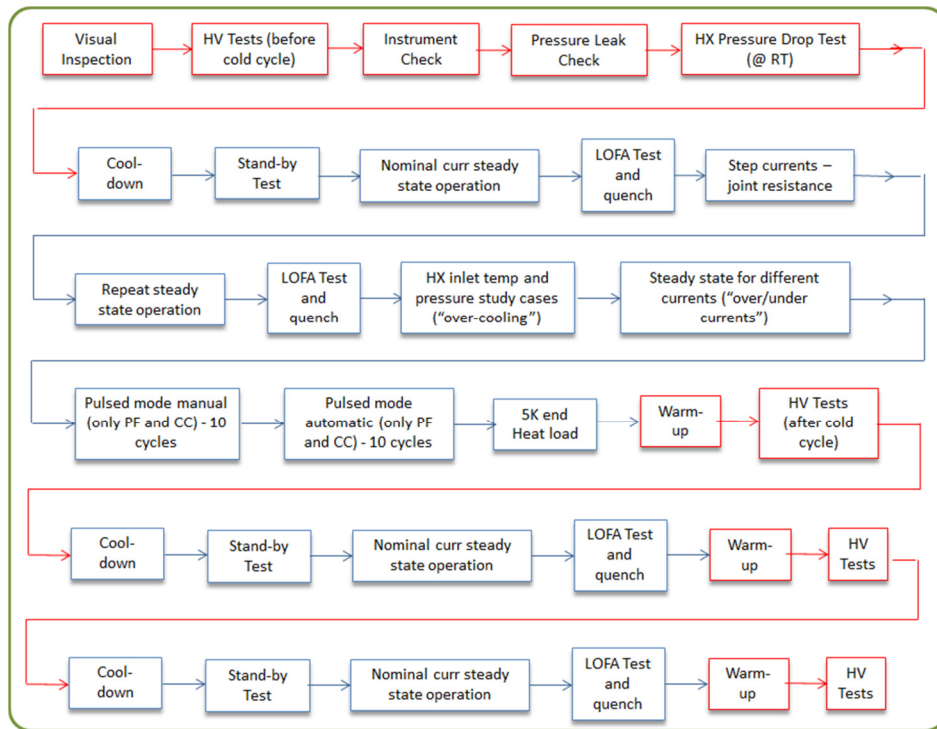


Figure 33: Prototype test flow.

HV tests, including hi-pot, partial discharge and Paschen tests were made before and after thermal cycling to check for degradation of the HV insulation.

Test Instrumentation and Data Channels

Figure 34 shows the location of the temperature sensors and V-taps on the CC current lead prototype. Most temperature sensors are of the Pt100 type¹⁰ (only exceptions are sensors 7 and 8

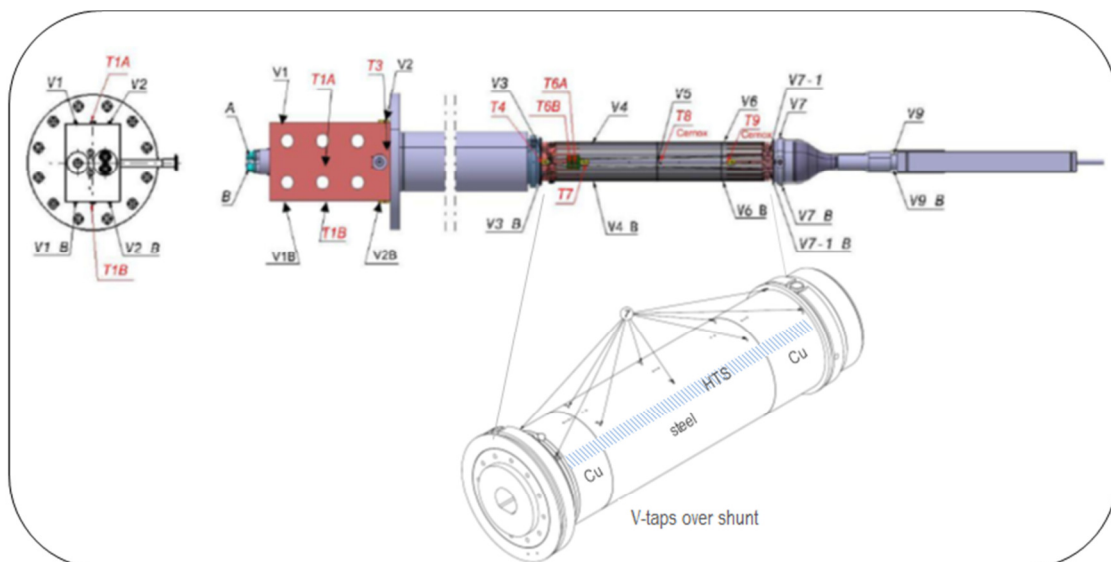


Figure 34: Instrumentation of ITER current lead. Not shown: auxiliary instruments in the CTB. See Table 4 for further explanation.

¹⁰ It was discovered during the (first) test campaign on the CC prototypes [ref 39], that the Siemens algorithm for read-out of the Pt100 sensors (according to IEC751) led to errors below ~ 70 K. An improved calibration by Lakeshore was therefore used in the sensor read-out chain.

Table 4: A selection from the process-variable channel list (full list has ~400 items).

Process Variable	Short	Explanation
MAG-HTS-CL:MI001-IT	Curr	Current
MAG-HTS-CL1/2:MT002-TT	T2	300 K exit temperature
MAG-HTS-CL1/2:MT001A/B-TT	T1A/B	Temp sensor middle of terminal block
MAG-HTS-CL1/2:MT003-TT	T3	Temp sensor start of terminal block (HX side)
MAG-HTS-CL1/2:MT006A/B-TT	T6A/B	Temperature HTS warm end
MAG-HTS-CL1/2:MT007A/B-TT	T7A/B	80% temperature sensor
nMAG-HTS-CL1/2:MT008-TT	T8	Temperature sensor middle of shunt (Cernox)
nMAG-HTS-CL1/2:MT009-TT	T9	Temperature sensor bottom of shunt (Cernox)
MAG-HTS-CL1/2:MP001-PT	P1	50 K supply pressure
MAG-HTS-CL1/2:MP002-PT	P2	300 K exit pressure
MAG-HTS-CL1/2:MT005-TT	T5	50 K supply temperature
MAG-HTS-CL1/2:MT002-TT	T2	300 K exit temperature
nMAG-HTS-CL1/2:MF-001-FT	HX-flow	300 K flow-rate (flow-controller)
MAG-HTS-CL1/2:VC001-CVZ	HX-valve	300 K exit valve opening in %
MAG-HTS-CL1/2:HT-001-LMN	RTheat	heater power in %
nMAG-HTS-CS:MP-004-PT	P4	5 K supply pressure
MAG-HTS-CS:MP003-PT	P3	Pressure sensor 5K out
nMAG-HTS-CS:MT-012-TT	T12	5 K supply temperature
n MAG-HTS-CS:MT010-TT	T10	5K exit temperature
nMAG-HTS-CS:MF-001-FT	SHe-a	5 K flow rate (cold Venturi)
MAG-HTS-CS:MF-001B-FT	SHe-b	5 K flow (warm flow-controller)
MAG-HTS-CL1/2:ME002A/B-ET	V2	V-drop over HX
MAG-HTS-CL1/2:ME004A/B-ET	V4	V-drop over shunt
MAG-HTS-CL1/2:ME008-ET	V8	V-drop over LTS linker and twin box joint
MAG-HTS-CL1/2:ME-003-ET	V3	V-drop shunt upper half
MAG-HTS-CL1/2:ME-005-ET	V5	V-drop HTS
MAG-HTS-CL1/2:ME-006-ET	V6	V-drop shunt bottom half

to measure the temperature profile along the lower section of the shunt, which are of the CERNOX type). Table 4 lists all the process variables which will be discussed in the following data plots.

Steady State Operation at different DC Currents

According to the test matrix (Figure 33) steady state tests were performed at different currents (typically 80%, 90%, 100% and 110% of the nominal). Figure 35 shows the performance

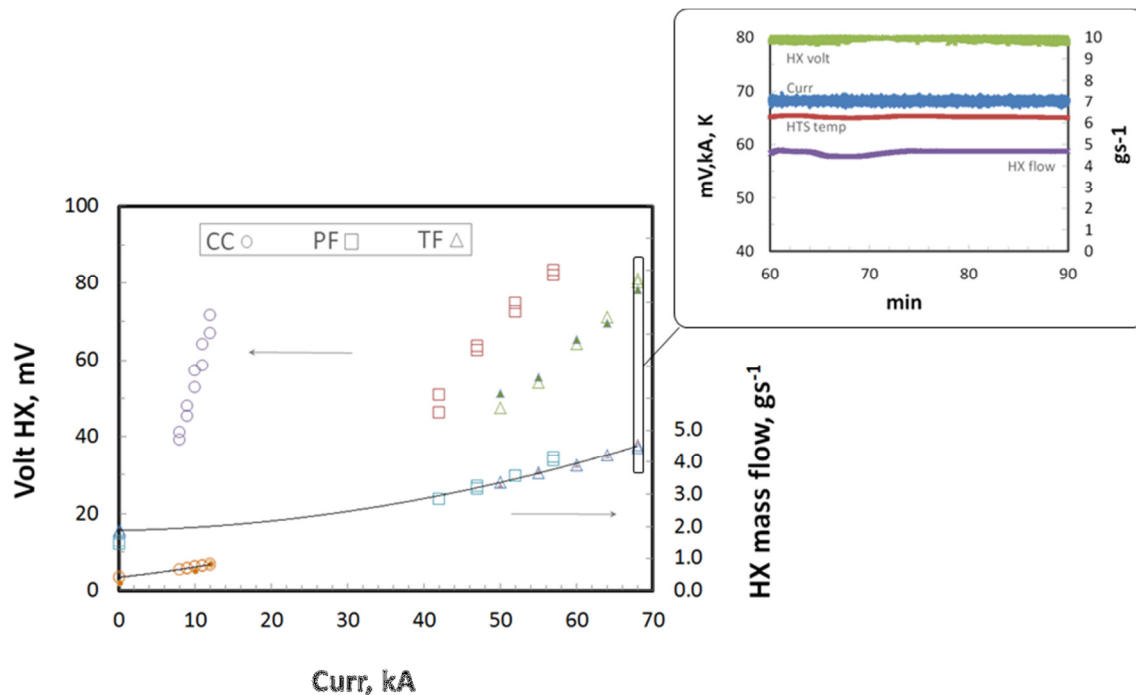


Figure 35: Prototype steady state HX voltage and mass-flow rate compared to model (full markers - CERN model for TF, model from [ref 44] for CC). Insert: example of steady state operation in the TF prototype at 68 kA.

parameters of the HX (voltage drop, steady state mass-flow) for the different currents. It was not possible to measure the HX temperature profile as it would have required highly invasive instrumentation, and the comparison with the model data was only performed for the integrated parameters: voltage drop, pressure drop and equilibrium mass flow rate (and outlet temperature, not shown here). In the case of the TF prototypes (the only one for which full length simulations were performed at CERN) the agreement of these parameters is good, as can be seen from Figure 35. Also for the CC mass-flow rates are predicted well by the model from [ref 44]. A minimum can normally be found when plotting the mass-flow-rate per unit current, which indicates the current for which the HX operates with the highest efficiency. The minimum is quite shallow, i.e. a wide range of currents is close to the optimum. As computed with the CERN 3D model of the HX discussed in section 3, the change of RRR value from the nominal ~ 80 to 185 (about the RRR value of the Cu stock used for the HX manufacture), increases the mass-flow requirement only by 0.1 g/s. The data shown in Figure 35 were computed for RRR=185. The pressure drop results are discussed separately below.

LOFA time, Over-Heating time and Temperature Margin

The effects of quenching the HTS were explored by taking data following a LOFA event, i.e. after the LOFA time (the time at full current it takes the lead to quench after interruption of the HX cooling). The measured LOFA and Over-Heating (OH) times for different steady state currents below and above nominal are shown in Figure 36. Thermal-cycling and multiple LOFA quenches did not impact on the performance of the leads, indicates good tolerance to local heating of HX and HTS/shunt assembly.

The quench is defined as occurring when the voltage exceeds 2 mV^{11} . The temperature T_6 of the

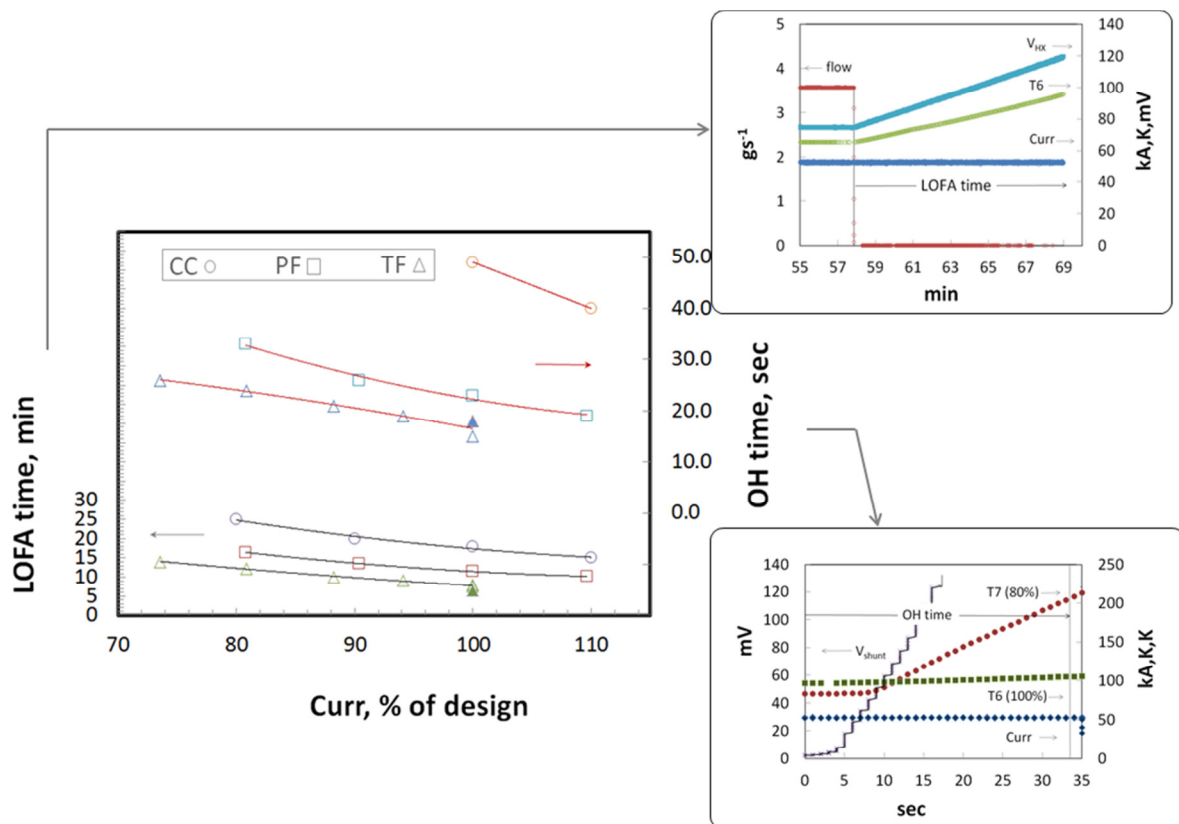


Figure 36: Prototype LOFA and over-heating time compared to IO model (full markers, without ITER stray field).

¹¹ The 0.1 or 1 $\mu\text{V}/\text{cm}$ criterion used for characterizing the tapes cannot be used in the leads (or in the ITER machine) as the power supply noise is much larger in this case.

top of the HTS at that time - typically the quench starts there as this is the warmest point of the HTS before the quench - can be considered as the quench temperature. When estimating the temp margin in the ITER condition the effect of an additional ~ 20 mT of magnetic field needs to be factored in (as discussed in section 3.2). The OH time is counted from the time the voltage crosses the 2 mV level to when the hot spot reaches 200 K (see secondary axis in Figure 36). Since for these tests the interlock system was disabled and the leads piloted manually it was not always possible to reach 200 K: for these cases the temperature profiles were extrapolated. In the CC prototypes the hot spot temperature sensors were located at the 90% and not the 80% mark as would have been more appropriate (100 % being the full-length of the HTS stacks – 310 mm - not counting the joints to the Cu). At the 90% mark the steel to Cu braze joint is underneath the HTS tape, so the temperature does not grow as fast as at the actual hot spot, located at $\sim 80\%$ (i.e. just below the end of the Cu/steel brazing overlap). This was taken into account in establishing the OH time for the CC.

Joint Resistances

The HX to HTS and HTS to LTS joint resistances were derived from the voltages V3 and V6 obtained for different current steps (Figure 37). The twin box joint resistance was obtained in a similar way from signal V8. As discussed in [ref 42] a series inductance was switched into the power supply circuit to reduce voltage noise and allow μV level measurements (the signal V8 is still too noisy to show in the example in Figure 37). Also not shown in Figure 37 are the data for the contact resistance between the RT terminal and the flexible, air-cooled interface busbars. As permanent V-taps were not installed, this measurement was performed manually using a complex procedure. First the current in each flexible was proportionally deduced from the total current and the voltage drop between the current lead terminal and each flexible top end (below the contact to the Al bus). These currents are then used to derive the resistance from the contact voltages between each flexible and the terminal. The total contact resistance was then computed assuming parallel connection. The resistances obtained in the prototype test campaigns are listed in the summary table (Table 6).

5 K End Heat Conduction

The heat conduction of the current lead was measured calorimetrically. After stabilizing the 5 K SHe cooling of the LTS loop (including the U-bend) for a given HTS top temperature (65, 80 and 100 K), the heat load was computed from the enthalpy difference (calculated from SHe temperature and pressure at the inlet/outlet) multiplied by the mass-flow. The mass-flow was

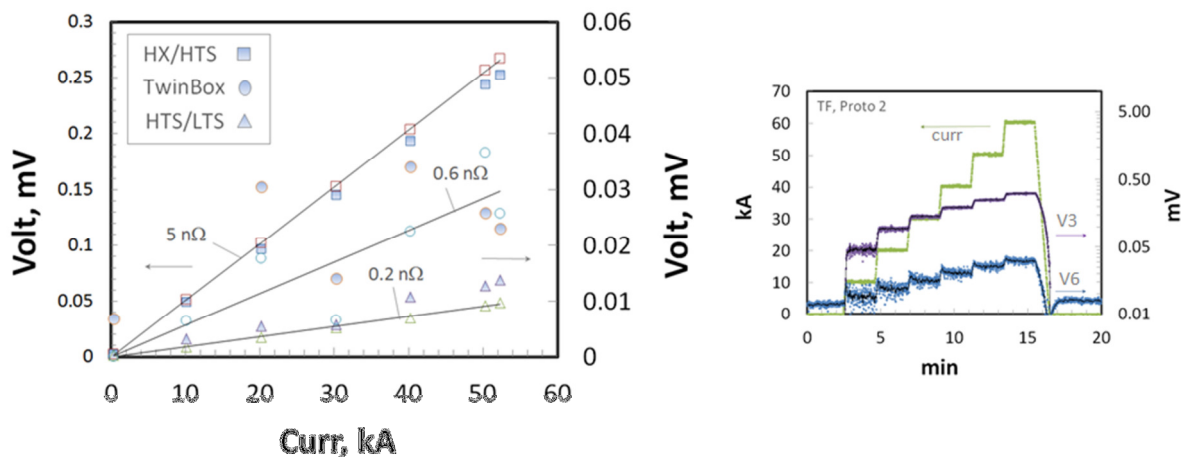


Figure 37: Left: V/I characteristics at different currents for PF prototype joint resistance measurements. Right: Example of raw data during a measurement (TF prototype). The signal V8 is too noisy to be plotted.

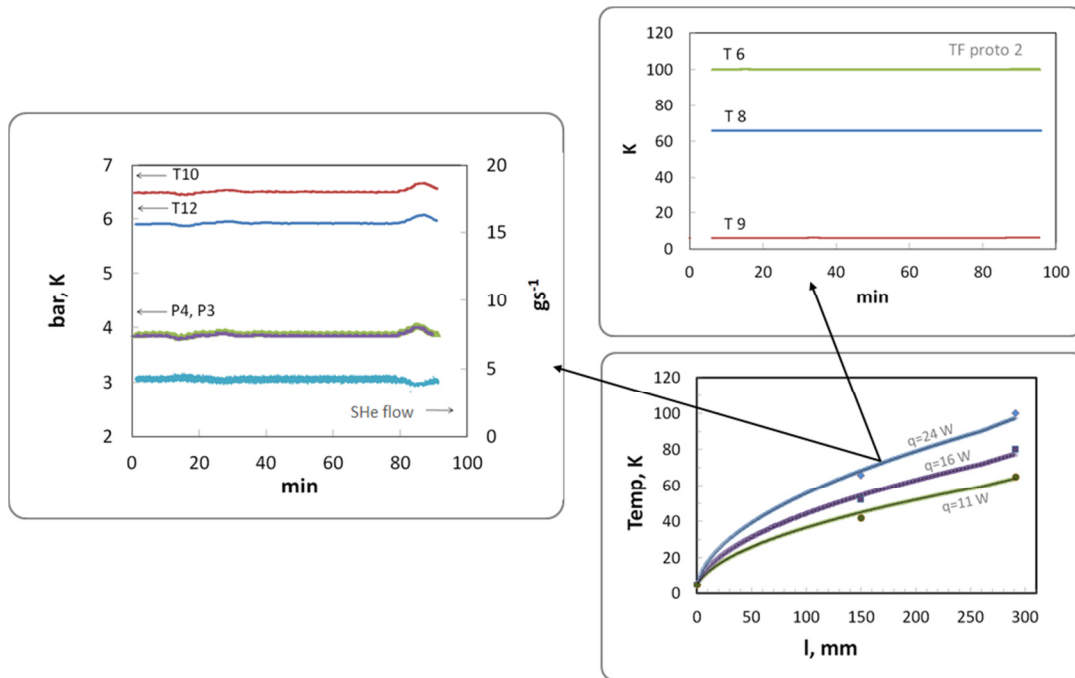


Figure 38: Left: Cold end heat load measurement for TF prototype. Left: data for heat conduction measurement by calorimetry, Right: temperature profile experimental data compared to the conduction model.

measured using a Hastings flow-controller after warming up the SHe in a large heat exchanger. Trials were also made to measure the flow at 5 K with a cold Venturi tube supplied by IO, but its precision was insufficient as it had been calibrated for a larger range of flow-rates (up to 30 g/s), and the measurement was less precise than with the flow-controller at room temperature. Since these tests were performed without current the TBJ resistances did not need to be taken into account. This technique applies to the entire 5 K loop and does not differentiate between the two leads (the total number is therefore divided by 2 to obtain the approximate individual heat load). To check that the heat conduction between the two leads was balanced, the heat load of each individual lead was also derived from the shunt temperature measurements (readings T_6 , T_8 and T_9 at the top, middle and bottom of the HTS) in combination with a temperature profile prediction as obtained from Equ (4). This method consists of plotting the recorded temperature readings and tuning the conduction heat load in the calculated temperature profile until it matches (see section 3.3). Figure 38 shows the result for one of TF prototypes. Although this method was less precise (due to a lack of measurement points), its consistency with the heat load value obtained from halving the 5 K circuit enthalpy, validates the calorimetric approach. The results of the calorimetric tests are further summarized in Table 6.

Over-Cooling Study

A key parameter, which was modified after completion of the current lead design, is the 50 K GHe supply condition for the resistive heat exchanger. Originally defined as 50 K (± 2 K), this was changed to a looser 40 K \div 52 K. Special, so-called “over-cooling” studies were conducted to explore the impact of lower inlet temperatures (and pressures) for the HX operation. The supply of 40 K GHe required a special operating mode for the refrigerator, evaporating at a high rate the LHe stored in the cold box to boost the cooling of the 50 K gas in one of the upstream counter-flow heat exchangers in the cooling chain. As summarized in Table 5 for the PF current lead prototypes, the following results emerged from this study. Provided the temperature difference between $T_{\text{he,in}}$ and $T_{\text{HTS-top}}$ remains 15 K, there is basically no difference in HX operation between 50 K and 40 K GHe supply temperature. The mass-flow is close to nominal and the lead operates stably. However, if this interval is increased, the mass-flow required drops and instability ensues. As shown in Figure 39 for the case of the PF prototype 1 (middle case), the HX voltage cannot

Table 5: Over-cooling cases in the PF prototypes.

Lead (PF)	Inlet temp (K)	Inlet press (bar)	HTS top (K)	HX flow (g/s)	HX volt (mV)	HX p-drop (bar)	stable/not-stable?
1/2	(K)	(bar)	(K)	(g/s)	(mV)	(bar)	
CL1	40	4	55	3.43	53.3	0.48	yes
CL1	40	4	65	2.87	-	-	no, test stopped at VHX=87.4 mV and growing
CL1	40	4	60	3.21	76	0.65	yes
CL1	40	3.5	55	3.44	53	0.54	yes
CL1	40	3	60	3.1	-	1	yes, but valve needs to be open 100%
CL2	40	4	55	3.63	48	-	yes
CL2	40	4	60	3.27	71.25	0.52	yes, but terminal took longer to converge (why?)
CL2	40	3.5	60	3.26	72.6	0.63	yes
CL2	40	3	55	-	-	-	no, at 100% open valve flow rate is limited to 2.9 g/s, T _{stop} rises to 60 K, possibly evolves into stable 40/60K case.

stabilize for the condition $T_{he,in} = 40$ K and $T_{HTS-top} = 65$ K, as the mass-flow (< 3 g/s) needed to set this temperature difference at the cold end of the HX is insufficient to cool its warm end. The HX voltage keeps growing (and would finally trigger the HX voltage interlock). This result, which was also verified for the TF prototypes, implies that operation in ITER with “looser” temperature tolerances at the inlet will require also changing the $T_{HTS-top}$ set-points for controlling mass-flow. For example, with 40 K operation the set-point should be $T_{HTS-top} = 55$ K. While the effect of lower inlet temperatures can be managed with an improved control algorithm, the effect of inlet pressure is more serious. The pressure drop in the HX increases when the inlet pressure is reduced, leading to a choking effect, i.e. at lower supply pressure the mass-flow through the HX is reduced, possibly leading to a thermal runaway. In the prototype experiments a similar effect was observed for pressure drops downstream of the leads (i.e. in the control valve and the flow-controller). As it can be expected that similar additional pressure drops occur in the ITER system, it is recommended that for operation the GHe supply pressure remains above ~ 3.8 bar (and below ~ 5 bar, as the safety valves for the current leads open at ~ 5.5 bar).

Pulsed Tests

While the ITER TF type current leads will operate in steady state, the PF-type and CC-type leads will operate in pulsed mode. Although not a criterion for their qualification, the prototypes were charged with a typical ITER pulse¹² current pattern to investigate their response. In the case of the PF-type leads, for example, the simulated pulse is more or less rectangular (steep flanks) with a

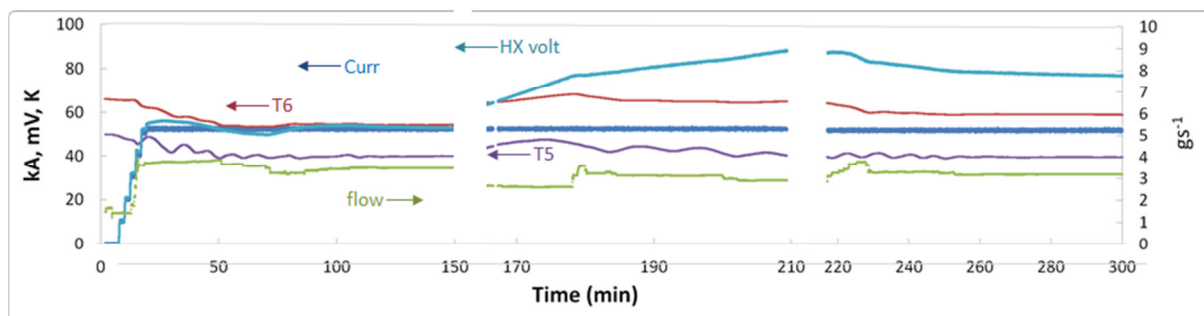


Figure 39: Results of the PF over-cooling study. Cases 1-3 from Table 5. Left: 4b/40K/55K (stable), Middle: 4b/40K/65K (not stable), Right: 4b/40K/60 K (stable).

¹² Note that the DC platform power-supply cannot supply negative currents, therefore the pulse was modified to have similar ramp rates and peak currents without excursions to negative currents.

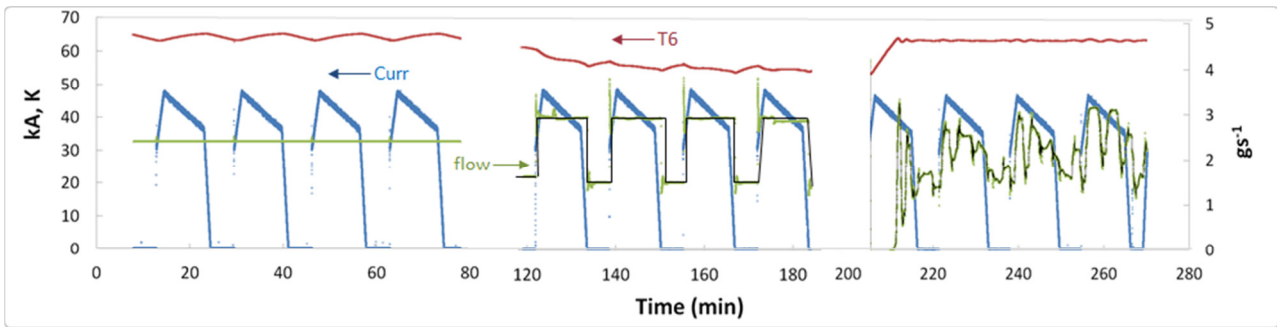


Figure 40: Three different flow control modes in the PF type current lead 1. Left: single flow (manual), Middle: "two-flow" (manual), Right: PID control (P=50, I=200, D=0).

linearly decreasing "plateau" (Figure 40). Three different current lead control modes were explored. The simplest consists of applying a constant flow in the HX calculated from the average current in the pulse pattern (note that the zero current flow rate is the "stand-by" flow rate). The so-called "two-flow" mode oscillates between the two flow modes, the stand-by flow at zero-current and the max-flow as needed for steady state operation at the pulse maximum current. Finally a PID control mode was also tested, varying the P, I and D parameters of the Siemens S7-300 control PLC. The thermal time constant of the leads was measured to be 30-60 min via open loop response tests (change of the valve settings and observation of system response). Accordingly, the I parameter was set to a larger 200 s, the D parameter to zero. In all three modes the HTS top temperature is reasonably controlled. There are, however, qualitative differences: the GHe room temperature control valve (located at the 300 K exhaust) valve works much harder in the automatic control mode. Possible implications of these results on the control algorithm will be discussed in section 5.

HX Pressure Drops

The HX pressure drops were usually obtained from the difference between the inlet and outlet absolute pressure measurements. This is not as accurate as the use of adequately chosen differential pressure gage, but was good enough, at least for the TF and PF-type leads, which have a substantial p-drop in nominal design conditions (~1 bar). The results of these measurements are shown in Figure 41 and listed in the summary table Table 6. As shown in the figure they also compare well to the prediction by the CERN model. The pressure drop in the CC leads, however, is very small, only a few kPa and not measurable from the absolute gauges used. In this case pressure drop measurements were conducted with GHe at room temperature and compared to those obtained in similar conditions in the CC HX mock-up (Figure 41, right graph). The goal of these comparisons was to evaluate possible by-pass gas flow, an issue which was

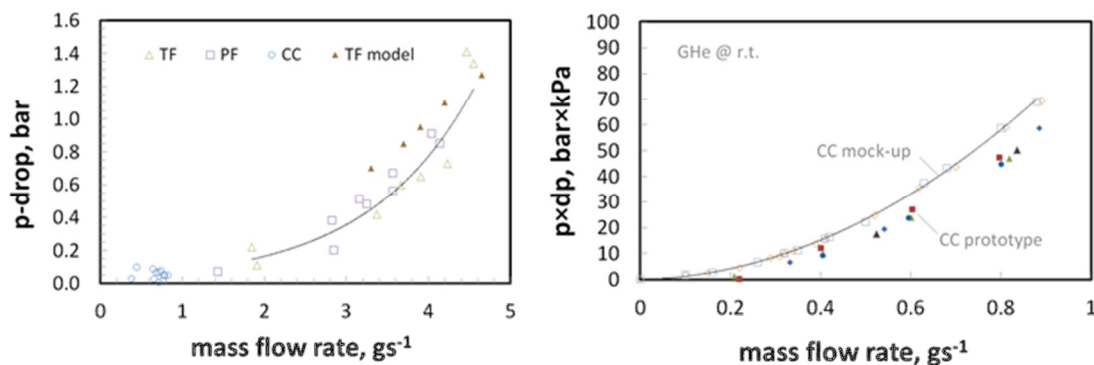


Figure 41: Pressure drops measured in nominal condition compared to model. Right: Comparison of pressure drop tests in CC prototypes and mock-ups with warm GHe.

believed to have affected some pre-prototype leads. No evidence of such by-pass flow was found, further corroborating the fact that geometrical data obtained on the HX cores and honed tubes during manufacturing were within specifications.

HV Tests

With the insulation design being finalized late, there was not time to insulate all prototypes and test them. It was therefore decided to test only one TF type lead (prototype 1) and one CC-type lead (prototype 2). These two prototypes were subjected to a full suite of HV measurements, including hi-pot, Partial Discharge (PD) and Paschen tests. The leads passed these tests, see results in Table 6. The table also gives some hi-pot and PD results for a PF-lead. This lead also passed a Paschen test, but the insulation design was not the final one, so the result is not relevant and is not reported.

A special HV test was conducted on the TF prototype 1, which consisted in filling the cavity created by the flange cylinder (which is normally filled with silicone rubber) with low pressure air. This essentially amounts to Paschen testing also the warm end of the insulation underneath the flange which normally does not need to be Paschen-tight. If it had failed, such a test would have revealed cracks in the glued interfaces between the HV insulation and the embedded ring glass layers and the insulating flange. The test was passed successfully indicating that the above interfaces were properly glued. Note that this section of the current lead normally operates above freezing temperatures, and cracking of the epoxy is not expected (unlike in cryogenic conditions).

Test Summary

A summary of the test results is presented in Table 6. The target values for the qualification parameters were all achieved or surpassed, with the exception of the RT terminal to interface busbar contact resistance. As noted in the table the HTS temperature margin, OH and LOFA times are as obtained directly from the tests and do not include the extra ~ 20 mT from the ITER stray field. In all these cases this effect will be absorbed in the ample margin found in the tests. More details on the CC prototype testing are discussed in [ref 43]. More details on the comparison to predictive analysis for the CC prototypes in [ref 44]. More details on the PF prototype testing are discussed in [ref 41]. Similarly as after the mock-ups, the current lead designs were further fine-tuned to take into account the results of the prototype tests. In particular the terminal blocks will be Ag coated to reduce the contact resistance to the flexible interface busbars. The twin-box joint design was also modified slightly to take into account the result of the qualification effort [ref 24]. Finally some adjustments were needed to optimize the interfaces. The instrumentation vacuum port was moved from the below the terminal to the instrumentation plug dome at its end for better access. Extra length will be left on all inlet and outlet pipes to allow circuit-by-circuit pressure testing during lead assembly into the feeder CTB. As decided recently the temperature sensors on the terminals will be optical, replacing the Pt100 type, with as

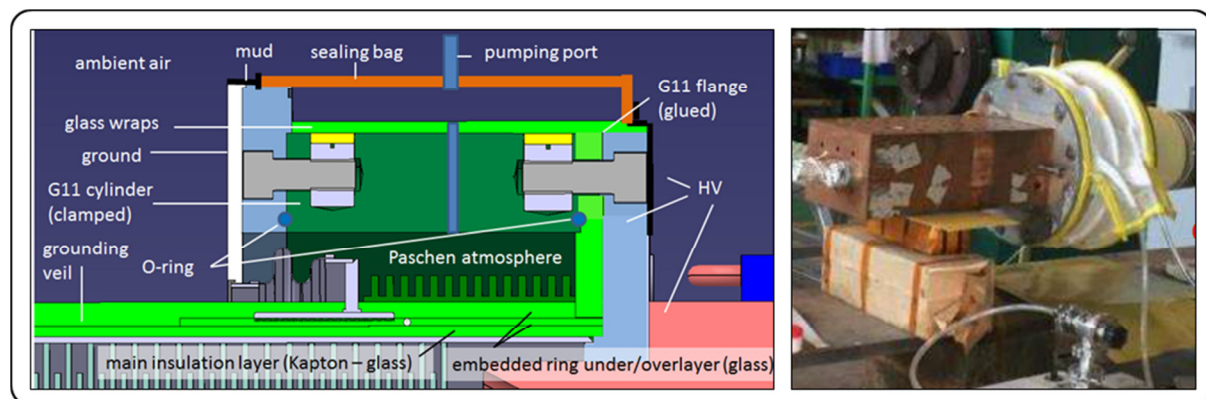


Figure 42: Special Paschen-test of the TF prototype flange assembly.

Table 6: Summary of the test-results for the three pairs of ITER HTS prototype current leads. See Table 3 for further details on the test conditions.

Qualification Parameter	TF I	TF II	PF I	PF II	CC I	CC II
Leak rate 50 K loop at test pressure (10^{-9} Pa·m ³ /s)	0.49	0.49	0.12	0.25	0.4	0.4
Leak rate 5 K loop at test pressure (10^{-9} Pa·m ³ /s)	0.83	0.83	0.27	0.27	0.28	0.28
Cold end heat load with HTS top at 65 K (W)	20/2	20/2	20/2	20/2	2*	N/A
Pressure drop in HX section at max DC curr (MPa)	0.13	0.125	0.066	0.065	0.005	0.007
50 K GHe steady state flow-rate at max DC curr (g/s)	4.6	4.7	3.6	3.6	0.7	0.6
50 K GHe steady state flow-rate at zero curr** (g/s)	1.9	1.9	1.55	1.45	0.3	0.3
Nominal operating voltage HX at max DC curr (mV)	77	76	74	73	60	63
Temp margin (2 mV crit) in ITER condition (K)***	27	27	31	31	30	30
LOFA time at max DC operation curr (2 mV crit) (s)***	480	480	690	690	1020	1020
HTS over-heating time (2 mV crit) (s)***	18	15	37	27	28	26
RT terminal and interface BB contact resistance (nΩ)	400	200	200	100	N/A	N/A
HX to HTS joint resistance (nΩ)	5.5	5.4	5.1	4.8	15.8	9.4
HTS to LTS joint resistance (nΩ)	0.1	0.4	0.2	0.3	0.4	0.4
HTS-CL to feeder busbar TB joint resistance (nΩ)	0.5	0.5	0.6	0.6	0.4	0.2
Resistance to ground in hi-pot test (GΩ)	3.3	N/A	30	N/A	50	4.5
Equivalent charge during PD test (nC)	5.0	N/A	2.5	N/A	N/A	0.1
Paschen test	pass	N/A	N/A	N/A	N/A	pass

* * obtained with the temperature profile method only; ** with 65 K at the HTS top; ***does not take into account the external stray field of ITER;

advantage that the signal conditioners are naturally insulated from HV through the optical fibers.

5. Next Steps

Phase III of the feeder PA is dedicated to the series production. Apart from defining the scope of the in-kind supply and giving a logistical framework for its implementation, the PA also aims to ensure that the ITER quality requirements are floated down to the domestic agency and its suppliers. The reason is that Tokamak components supplied by the different domestic agencies conform to the same standards and to the requirements of the local (French) authorities. It was a major undertaking to set up the QA framework specified in the PA. But it is expected that this investment will prevent major cost and schedule overruns during the series manufacturing.

5.1. Quality Assurance for Series Manufacturing

All test equipment must have valid calibration certificates. Operators (welders, NDT, ..) need to be qualified with up-to-date certificates. All critical manufacturing processes, and in particular the welding, brazing, soldering and insulation steps, will be implemented according to the PED. Materials will be fully tested according to codes as discussed in the introduction of section 4. Shop-floor procedures for all critical processes, specifying in detail the Quality Control (QC) to be performed after each manufacturing step, need to be approved by CNDA and IO prior to the start of manufacturing. The suppliers also submit for approval Manufacturing and Inspection Plans (MIP) to seamlessly cover the manufacture, allowing managing the production process - important for schedule issues. The IO supplied Manufacturing Database (MDB), [ref 45], is structured around these MIPs. In MDB each production step is processed (mostly by the DA) upon supplier clearance of the QC record for the specific step. MDB also provides a procedural framework for the management of deviations and non-conformances. Finally the MIP also allows the DA and IO to define which operation requires witnessing or special clearance (hold-points). In total there are approximately 800 quality documents for the three types of current leads (specifications, drawings, procedures, MIPs, etc.). Not to mention the tens of thousands of QC records that will be uploaded during the series production over the next years.

Full penetration welds are prescribed wherever possible, but volumetric NDE (Non Destructive Examination) is not applicable for most welds in the complex geometry of the HTS leads. The suppliers have also decided that most of the welds will be done manually (except for the EBW). For some specific welds a Production Proof Sampling (PPS) scheme will be set-up in lieu of volumetric testing. For the others a combination of dye Penetrant Testing (PT) and/or Ultra-sonic Testing (UT) and leak checking (10^{-9} Pa-m³/s criterion) will be applied. Particular emphasis will be put on ensuring that only qualified welders perform the work and that they follow strictly the qualified procedures. This is supplemented by periodic destructive testing of the PPS. This reinforced supervision also requires witnessing of all these manufacturing steps by CNDA/IO and/or selected third-party inspectors representing them.

Most importantly – *all* HTS current leads will be cold tested, similarly (although with a streamlined test program) to the prototypes. Recently a test cryostat for the PF-type current leads (with its own instrumentation and control cubicles) was added to the two cryostats already available for the CC and TF-type current leads (which were used in phase II) [ref 46]. Although the three cryostats will share the same cryo-plant and the TF and PF system share the 80 kA “DC platform” power supply, this arrangement will allow separate assembly and dis-assembly of the current leads during series production, significantly reducing the turn-around time for series lead testing.

5.2. Integrated System Test

The so-called “S-bend mock-up” is a systems test of the feeder box containing the HTS current leads and the so-called “S-bends”, all according to the final design. It is presently in the final stages of preparation. In this test the HTS lead will be thermally cycled and mechanically loaded (by pulling on the S-bends) to simulate the feeder operation, followed by leak and HV testing to assess a possible impact of the operation on the lead (and other feeder components) integrity (in particular its insulation). The results of these tests will be reported elsewhere.

5.3. Some Thoughts on Operation

There will be two main control loops for operating the HTS current leads in the ITER device. One is the heater power regulation for the room temperature terminals. The heater power will be regulated by conventional PID control aiming to keep the terminal temperature always above 0°C to prevent condensation (note the current lead terminals are in a dry air environment with a nominal dew point of -40°C). The more important control loop concerns the control of the temperature of the HTS shunt warm end. A target temperature and variation are defined and a PLC will regulate the GHe exhaust valve opening such as to vary the GHe flow in the HX to achieve this target. This is complicated by the larger range of GHe supply temperatures now proposed for the ITER cryo-system operation. A particularity of the ITER leads, however, is that they will be equipped with flow-meters. The well-established correlation of the HX equilibrium flow-rate with operating current (see for example Figure 35), enables a control scheme in which the valve is operated to produce a flow-rate consistent with the actual operating current as obtained from this correlation. The pulsed mode measurements discussed in section 4.3 have already shown that a feed-forward scheme setting the flow to a value calculated from the “average current” in a pulse is sufficient to provide reasonably good temperature control (Figure 40). The long (>30 min) thermal response time of the leads is certainly helpful there. Furthermore, as was shown in the over-cooling studies discussed in section 4.3 the HTS top temperature automatically regulates itself to the desired $T_{He,in}+15$ K, when the flow-rate is correctly matched to the current, whatever the GHe inlet temperature (this certainly applies to the inlet temperature range now considered as shown in Figure 39). This scheme would therefore not

only be simpler than a PID regulation (and make the valves work less “hard”), but also address the issue of the wider range of the GHe supply temperatures.

Following the successful test of the various interlock parameters in the prototype tests, the interlocks must now be properly fine-tuned to find a suitable compromise between current lead operation and machine requirements. It must be shown, for example, that the 2 mV threshold applied for the HTS quench protection can be resolved in the noisier machine environment. The prototype tests, however, have shown that there is considerable margin for especially the CC and PF current lead types, possibly allowing a higher detection threshold (see OH times in Table 6).

A related problem would concern the temperature read-out of the Pt100 sensors located at the warm end of the HTS at the current lead potential (up to 30 kV) - the common mode rejection of the differential amplifier would need to be state-of-the-art to resolve the 0.1 Volts level for read-out. This issue is “naturally” resolved for the optical temperature sensors on the terminal, however. In the worst case, as discussed above, a flow/current control mode alone would suffice to operate the leads even in the absence of HTS top temperature data.

6. Conclusions

HTS current leads, together with superconducting magnets, are one of the enabling technologies for large scale fusion power plants, as they reduce the input power requirement for plant operation. The development of high current HTS leads, which was first driven by the high energy physics accelerator community, is now being pushed by the fusion magnetic confinement community towards larger currents. At 68 kA the ITER TF type HTS current leads will be the largest ever operated. A considerable effort was made during the last ten years to first design and then prototype and qualify the HTS current leads for the ITER project. Great care was applied to ensure their design will be safe in operation. The HTS represents about 25% of the cost of a current lead, and the total additional investment compared to using non-HTS conventional leads is several M€, but this will be quickly amortized by savings in the cost of cooling, which are of the order of 1 M€/year.

Acknowledgements

This work would not have been possible without the major contributions of:

Y. Bi, K. Ding, Q. Du, Q. Han, X. Huang, J. Li, C. Liu, C.L. Liu, K. Lu, Y. Song, Q. Ran, T. Zhou
of ASIPP,

A. Ballarino, B. Bordini, T. Miani, M. Sitko, T. Spina, S. Landeslag of CERN,
O. Chaveau, N. Clayton, A. Devred, C.Y. Gung, D. Kaverin, S. Lee, U. Lemarchand, M. Matos-
Torres, F. Michel, N. Mitchell, R. Piccin, N. Sato, M. Su, N. Utzel, A. Vergara, P. Vertongen of
IO,

and *E.Niu (CNDA), R. Heller (KIT), T. Ichihara (Fusac), V. Tanchuk (Efremov), T. Taylor*
(ATScientific), *S.Yamada (NIFS) and Y. Yang (Univ. Southampton)*

The authors are also particularly grateful to the staff of the Juneng and Keye companies, whose tireless efforts were certainly rewarded with the successful qualification of the HTS leads for ITER!

Disclaimer

The views and opinions expressed herein do not necessarily reflect those of the ITER Organization.

7. References

- [1] Bauer P et al 2012 IEEE Trans Appl SC Vol. 22 No 3
- [2] Taylor T 1999 IEEE Trans Appl SC Vol 9 p 412-415
- [3] Ballarino A 1999 IEEE Trans Appl SC Vol 9 p 523–526
- [4] Heller R et al 2004 IEEE Trans Appl SC Vol 14 No 2 p 1774
- [5] Heller R et al 2005 IEEE Trans Appl SC Vol 15 No 2 p 1496,
- [6] Heller R Fietz WH Lietzow R Tanna VLVostner A Wesche R Zahn GR 2006 IEEE Trans Appl SC Vol 16 No 2 p 823
- [7] Fietz W Heller R Lietzowa R Tanna VL Zahn G Wesche R Salpietro E Vostner A 2005 21st IEEE/NPS Symposium on Fusion Engineering
- [8] Heller R 2009 IEEE Trans Appl SC Vol 19 No 3 p 1504
- [9] Bi Y Chen X Ma D Liu X Wu S Li J 2005 Proceedings of ICEC 20 p 681
- [10] Bauer P et al 2009 IEEE Trans Appl SC Vol 19 No 3 p 1500
- [11] Bi Y et al 2010 IEEE Trans Appl SC Vol 20 No 3 p 1718
- [12] Ding K Bi Y Yu J Zhou T Liu CL Lin X Shen G Song Y 2010 IEEE Trans Appl SC Vol 20 No 3 p 1729
- [13] Huang X Bi Y Cheng Y Lu L Wang C Shen G Song Y 2010 IEEE Trans Appl SC Vol 20 No 3 p 1722
- [14] Bauer P et al 2011 IEEE Trans Appl SC Vol 21 No 3 p 1074
- [15] Liu C et al 2012 IEEE Trans Appl SC Vol 22 No 3
- [16] Ding K et al 2012 Physics Procedia 36 p 931 – 936
- [17] Zhou T Ding K Liu CL Bi Y Song Y 2015 IEEE Trans Appl SC Vol 25 No 2
- [16] Heller R Fietz WH Kienzler A Lietzow R 2009 IEEE Trans Appl SC Vol 19 No 3 p 2202
- [19] Wesche R Heller R Bruzzone P Fietz WH Lietzow R Vostner A 2007 Fusion Eng and Design 82 p 1385
- [20] Heller R Fink S Friesinger G Kienzler A Lingor A Schleinkofer G Suesser M Ulbricht A Wuechner F Zahn G 2001 Cryogenics 41 p 201-211
- [21] Drotzinger S Fietz WH Heller R Jung A 2016 IEEE Trans Appl SC Vol 26 No 2
- [22] Kovalev I A Surin M I Naumov A V Novikov M S Novikov S I Ilin A A Polyakov A V Scherbakov V I Shutova D I 2017 Cryogenics Vol 85 p 71
- [23] Taylor T 2012 IEEE Trans Appl SC Vol 22 No 3
- [24] Ilin Y et al 2016 IEEE Trans Appl SC Vol 26 No 4
- [25] Calvi M Bauer P Bessette D Cau F Marinucci C Bruzzone PL 2010 IEEE Trans SC Vol 20 No 3 p 407
- [26] Knaster J Rajainmaki H Evans D Losasso M 2013 IEEE Trans SC Vol 23 No 3
- [27] Sitko M Bordini B Ballarino A Bauer P Devred A 2013 IEEE Trans Appl Supercond Vol 23 No 3
- [28] Hu L et al 2003 Physica C 386 p 131
- [29] Wesche R Fuchs AM 1994 Cryogenics Vol 34 No 2 p 145
- [30] Rizzo E Heller R Savoldi Richard L Zanino R 2012 IEEE Trans Appl Supercond Vol 22 No 3
- [31] Langeslag S A E Sgobba S Libeyre P Gung C Y 2015 Physics Procedia 67 p 1036
- [32] Bauer P Ding K Gung CY Ichihara T Niu E Shen G Taylor T Vertongen P Zhou T 2013 IEEE Trans Appl Supercond Vol 23 No 3
- [33] Zhou T Lu K Ran Q Ding K Feng HS Wu H Liu CL Song Y Niu E Bauer P 2014 IEEE Trans Appl Supercond Vol 24 No 3
- [34] Zhou T Lu K Ran Q Ding K Feng HS Wu H Liu CL Song Y Niu E Bauer P Devred A 2015 Fusion Eng and Design 96–97 p 388
- [35] Bauer P Ballarino A Bordini B Devred A Ding K Niu E Sitko M Taylor T Yang Y Zhou T 2015 IOP Conf. Series: Materials Science and Engineering 101
- [36] Clayton N Crouchen M Devred A Evans D Gung CY Lathwell I 2017 Cryogenics Vol 83 p 64
- [37] Huang X et al 2017 Fusion Eng and Design Vol 114 p 13
- [38] Fietz W H Fink S Kraft G Scheller H Urbach E,Zwecker V 2013 IEEE Trans Appl Supercond Vol 23 No 3
- [39] Zhou T et al 2016 IEEE Trans Appl SC Vol 26 No 6
- [40] Zhou T Ding K Liu C Bi Y Song Y 2015 IEEE Trans Appl SC Vol 25 No 2
- [41] Ding K Liu C Zhou T Du Q Dong Y Lu K Song Y Niu E Bauer P - Test Results of ITER 52-kA HTS Current Lead Prototypes, submitted for publication SOFE 2017
- [42] Ding K Liu CL Bi Y Feng HS Du Q Zhou T Lu K Song Y Xu L 2016 IEEE Trans Appl Supercond Vol 26 No 3
- [43] Ding K et al 2016 IEEE Trans Appl SC Vol 26 No 4
- [44] Zappatore A Heller R Bauer P Savoldi L Zanino R 2016 Cryogenics 80 Part 3 p 325
- [45] Bevallard G Seo K Savary F Devred A Patel A Capuano C Bartels HW Gardner M Mitchell N 2012 IEEE Trans Appl Supercond Vol 22 No 3
- [46] Liu C Ding K Du Q Dong Y Wang J Lu K Song Y Niu E Bauer P – Test System upgrade for the ITER Current Lead Series Production at ASIPP, submitted for publication SOFE 2017